Experimental Observations of Broadband Magnetic Fluctuations in ASDEX

L. Giannone

ASDEX, NI, ICRH and Pellet teams

IPP III/138

June 1989

MAX-PLANCK-INSTITUT FÜR PLASMAPHYSIK

8046 GARCHING BEI MÜNCHEN

MAX-PLANCK-INSTITUT FÜR PLASMAPHYSIK

GARCHING BEI MÜNCHEN

Experimental Observations of Broadband Magnetic Fluctuations in ASDEX

L. Giannone

ASDEX, NI, ICRH and Pellet teams

IPP III/138 June 1989

Die nachstehende Arbeit wurde im Rahmen des Vertrages zwischen dem Max-Planck-Institut für Plasmaphysik und der Europäischen Atomgemeinschaft über die Zusammenarbeit auf dem Gebiete der Plasmaphysik durchgeführt.

CONTENTS

1. INTRODUCTION

The existence of anomalous electron transport in tokamaks is the motivation for experiments which seek to explain this phenomenon in terms of enhanced particle and energy transport produced by fluctuations in the plasma /1/.

Measurements by Langmuir probes support the hypothesis that electrostatic fluctuations are reponsible for enhanced particle transport in the edge plasma /2/. The correlation between broadband magnetic fluctuation amplitude and the inverse of energy confinement time /3,4/ would suggest that this enhancement is a result of the coupling of transport across the magnetic field to the rapid transport along the magnetic field when the fluctuations are of sufficient amplitude to destroy magnetic flux surfaces. The main objection to this viewpoint is the dependence of broadband fluctuations on edge plasma conditions reported on TFTR /5/, where gas puffing in an ohmically heated discharge was found to cause a significant decrease of the broadband magnetic fluctuation amplitude. Also instability theory shows that values of poloidal beta greater than one are necessary to excite electromagnetic instabilities /6/ and generate magnetic fluctuations of sufficient amplitude to produce enhanced transport /7,8,9/. A systematic study of broadband magnetic fluctuations in ASDEX was undertaken in order that definite conclusions about the opposing viewpoints could be drawn.

Broadband magnetic fluctuations in ASDEX were previously studied with Mirnov coils which are fixed at a distance of 12 cm from the separatrix. This report documents the extension of that work. The magnetic probe is mounted on a pneumatically driven manipulator. This allows the radial postion of the probe to be scanned during the discharge or a

stationary probe to be fixed at a chosen distance from the separatrix. Estimates of the poloidal mode number, m, from the radial decay of the magnetic fluctuation amplitude are therefore possible. In previous experiments m was estimated from measurements with a poloidal array of probes. The radial distance of each coil of the array to the plasma boundary was different and this allowed the radial decay of the magnetic fluctuation amplitude to be plotted /10,11/.

Magnetic probes in major tokamaks have been usually positioned close to the vessel wall and strongly shielded. Signal - to - noise ratios then deteriorate above a few hundred kilohertz /4/. The probe system on ASDEX can provide a measurable response at 1 MHz in Ohmic discharges. This feature proves to be of particular importance in the study of the IOC mode /12/, the H - mode and plasma discharges with neutral beam injection and ion cyclotron resonance heating (ICRH).

Measurements on ASDEX indicate that edge plasma conditions play a role in determining the level of broadband magnetic fluctuations. This was inferred from observations of a perturbation of the magnetic fluctuation amplitude coincident with the arrival of the heat pulse induced by a sawtooth crash. The measurement of an $m \approx 25$ mode in the toroidal field component of the fluctuating magnetic field in the vicinity of the separatrix in Ohmic discharges and the behaviour of this component during the H - mode adds further weight to the connection between edge plasma conditions and broadband magnetic fluctuations.

2. THEORY

The low frequency instabilities ($\omega < \omega_{ci}$) of an inhomogeneous, finite beta plasma in a magnetic field /13/ may enhance particle and energy transport and give rise to the anomalously large values of electron thermal conductivity, χ_e, and diffusion coefficient, D, commonly observed in tokamaks /1/. Broadband fluctuations of density, electric field and magnetic field in this frequency range are routinely measured in tokamaks and these fluctuations are considered to represent the non-linear saturated state of one of the two classes of instability present.

The simplest theoretical treatment of the stability of an inhomogeneous, finite beta plasma in a magnetic field /14,15/ assumes that a uniform magnetic field, B_o, is directed along the z-axis, a density gradient in the direction of the x-axis is supported, and the plasma temperature, T, is constant. The excitation of waves analagous to the Alfven wave and ion acoustic wave of a homogeneous plasma /16/ are derived from the set of two-fluid equations.

From the pressure balance equation :

$$\nabla P = j \times \underline{B} \qquad (2.1)$$

it is necessary that an electron drift exists to support the pressure gradient. This drift is perpendicular to the magnetic field and the density gradient :

$$\frac{\partial P}{\partial x} = j_y B_o \qquad (2.2)$$

$$T \frac{\partial n}{\partial x} = - (n e v_{de}) B_o \qquad (2.3)$$

$$v_{de} = T / (e L_n B_o) \qquad (2.4)$$

where v_{de} = the electron diamagnetic drift velocity

$L_n = | n / (\partial n/\partial x) |$ = the density scale length.

and T is expressed in energy units.

Two wave types may be identified from the dispersion relations. The drift wave consists of an accelerated and a retarded ion acoustic mode :

$$\omega = - 1/2 \; (\; \omega_{*e} \pm (\; \omega_{*e}^2 + 4 \; k_z^2 \; c_s^2 \;)^{1/2} \;) \qquad (2.5)$$

where $\omega_{*e} = k_y \; v_{de}$ = the electron diamagnetic drift frequency

$c_s = (\; T/m_i \;)^{1/2}$ = the ion acoustic speed

Drift wave instabilities may enhance particle and energy transport across the magnetic field through a correlation between electron density and electric field fluctuations /1/.

The drift-Alfven wave consists of an accelerated and a retarded Alfven mode :

$$\omega = 1/2 \; (\; \omega_{*e} \pm (\; \omega_{*e}^2 + 4 \; k_z^2 \; v_A^2 \;)^{1/2} \;) \qquad (2.6)$$

where $v_A = B_o \; / \; (\mu_o \; n \; m_i \;)^{1/2}$ = the Alfven speed

Electromagnetic instabilities may enhance particle and energy transport through the coupling of transport across the magnetic field to the more rapid transport along the magnetic field. The stochastic magnetic field fluctuations associated with drift-Alfven waves destroy magnetic flux surfaces /1/. The disperion relations of equations (2.5) and (2.6) are plotted in Fig. 1.

More sophisicated treatments include the effects of finite resistivity /17/, magnetic field curvature /18/, electron temperature gradients /19/, or ion temperature gradients /20/. The inclusion of these effects gives rise to

a variety of waves related to the drift or drift-Alfven wave. The microtearing mode correponds to the drift-Alfven wave mode in the limit $(k_y\rho_i)^2 << 1$ /19/. The η_i mode is related to the retarded ion acoustic wave which propagates in the direction of the ion drift.

The identification of the mode reponsible for anomalous electron transport in tokamaks is the goal of fluctuation experiments. Experiments with Langmuir probes in the edge plasma /2/ lend support to the view that electrostatic modes enhance particle and energy transport. The contribution of magnetic fluctuations to anomalous electron transport has also been theoretically treated /7,8,9/ and compared to experimental measurements /9,21/. The enhancement of χ_e in this experiment, was accounted for by magnetic fluctuation induced transport rather than electrostatic induced transport. Values of poloidal beta greater than one in neutral beam heated discharges were obtained in these experiments.

A better understanding of anomalous transport is relevant to the next generation of tokamaks which will seek to achieve ignition. Further measurements of broadband magnetic fluctuations in tokamaks, which are aimed at defining their role in anomalous transport, are then of interest.

3. EXPERIMENTAL APPARATUS

A new set of coils, mounted on a pneumatically driven manipulator, has been recently installed on ASDEX. Each coil is wound with 46 turns of copper wire on a 2.2 cm x 2.2 cm alumina former (NA = 2.2 x 10^{-2} m^2). The coils are wound with two layers, each of 23 turns, to minimise any contributions to the measured signal by components perpendicular to the desired component. Coils wound with only a single layer possess a single turn oriented perpendicularly to the main set of windings.

The radial, poloidal and toroidal components of the fluctuating magnetic field may be measured simultaneously. The 3 coils of each probe assembly are wound on a single former. Two assemblies of 3 coils are mounted directly upon one another with a separation of 3.0 cm in the radial direction between the axes of the coils. A schematic diagram of the experimental arrangement is shown in Fig. 2. A slotted graphite shield surrounds the probe to provide electrostatic shielding of the coils, while still allowing penetration of the magnetic field. The direct impingement of plasma upon the coils is prevented by an alumina cap.

Further minimisation of capacitive coupling to the probe coils is afforded by a transformer. A passive high pass filter is employed to attenuate the dominant coherent magnetic fluctuations due to Mirnov oscillations. Typical values of the frequency of Mirnov oscillations in ASDEX range from 5 kHz in Ohmic discharges up to 30 kHz in neutral beam heated discharges. The broadband signal is then amplified with a gain of up to 200 in Ohmic discharges by a Tektronix AM 502 differential amplifier.

The magnetic probe system was calibrated using a Helmholtz coil.

At sufficiently low frequencies the self inductance of the probe may be neglected. The output voltage, ε, of the coil is then related to the area times number of turns, NA, and the amplitude of the sinusoidal magnetic field, B, by:

$$\varepsilon = G\ NA\ \omega\ B \qquad (3.1)$$

where G is a product of the amplifier gain and high pass filter response at each frequency. Measurements of ε at known B for different frequencies yield the probe calibration curve in Fig. 3. For the purposes of calibration an effective GNA value is calculated even though the assumption that the self inductance of the probe may be neglected is no longer valid at frequencies greater than 100 kHz.

The amplifier output is then monitored by an analogue to digital converter, a spectrum analyser or a frequency comb. A typical signal is shown in Fig. 4. The frequency comb /3,5/ consists of a splitter, whose output is processed by a set of 8 bandpass filters. The RMS amplitude of the coil output at 8 frequencies in the range 30 kHz to 1 MHz are simultaneously measured. The bandwidth of each channel of the frequency comb was chosen so that $\Delta f/f = 0.1$. The central frequency of each channel was chosen to cover the frequency range of interest with a geometrical progression between successive channels ($f_n/f_{n-1} = 1.65$).

The calibration of each channel by measurements of the output for sinusoidal inputs at various amplitudes, allows non-linearities in the response of the frequency comb to be corrected. The power spectrum in units of

T^2/Hz is obtained by applying this response function in combination with the response function of the probe to convert the output voltage of the frequency comb into a magnetic field amplitude. This amplitude is squared and divided by the bandwidth of the bandpass filter to obtain the power per unit bandwidth in each channel.

The lower limit in frequency range was chosen to avoid contributions by the higher harmonics of the Mirnov oscillations in an Ohmic discharge. The upper limit was determined by the upper 3 dB point of the amplifiers. In Fig. 5 a schematic diagram of the electronics connected to the probe system is displayed. The response of the frequency comb to a sinusoidal input which is swept in frequency is shown in Fig. 6. This displays the capability of the frequency comb to measure each frequency component of the broadband input independently.

4. RADIAL DECAY OF MAGNETIC FLUCTUATIONS

A quantitive analysis of the radial decay of broadband magnetic fluctuations begins by considering the perturbed magnetic field, $\underline{b}$, in a vacuum region. This is governed by Maxwell's equations :

$$\nabla \times \underline{b} = 0$$

$$\nabla \cdot \underline{b} = 0 \qquad (4.1)$$

Perturbations of the following form in cylindrical geometry are assumed :

$$\underline{b} = \underline{b}(r) \quad \exp (i (m\theta - k_z z)) \qquad (4.2)$$

Assuming an infinite toroidal wavelength so that $k_z = 0$, leads to the following differential equation for the radial component of $\underline{b}$:

$$r^2 \frac{d^2(r b_r)}{dr^2} + r \frac{d(r b_r)}{dr} - m^2 (r b_r) = 0 \qquad (4.3)$$

The two solutions $r\, b_r = c_1\, r^m$ and $r\, b_r = c_2\, r^{-m}$ together with the boundary condition $b_r\,(r_w) = 0$ at the conducting wall located at $r = r_w$ yields :

$$b_z = 0$$

$$i\, b_\theta = - c/r^{(m+1)} \left(1 + (r/r_w)^{2m} \right) \qquad (4.4)$$

$$b_r = \quad c/r^{(m+1)} \left(1 - (r/r_w)^{2m} \right)$$

where c is an arbitrary constant. When the conducting wall is at an infinite distance from the plasma, then the familiar decay law is recovered :

$$|b_r| = |b_\theta| = c/r^{(m+1)} \qquad (4.5)$$

The decay of the magnetic fluctuation amplitude in the presence of a conducting wall at a finite distance from the plasma with $k_z \neq 0$ has been previously considered /22/. The differential equation for the axial component of $\underline{b}$ with $k_z \neq 0$ is :

$$r^2 \frac{d^2 b_z}{dr} + r \frac{db_z}{dr} + (k_z^2 r^2 - m^2) b_z = 0 \qquad (4.6)$$

where $k_z = n/R$. The solution is a linear combination of the modified Bessel functions $I_m(k_z r)$ and $K_m(k_z r)$. Then :

$$b_z = k_z (c_1 I_m(k_z r) + c_2 K_m(k_z r))$$

$$b_\theta = - m/r (c_1 I_m(k_z r) + c_2 K_m(k_z r)) \qquad (4.7)$$

$$- i b_r = k_z (c_1 I_m'(k_z r) + c_2 K_m'(k_z r))$$

with the boundary condition $b_r (r_w) = 0$ determining the constants c_1 and c_2. In practice a number of modes will be simultaneously unstable. When modes of the same amplitude are located at the same radial position then those modes with the lowest m predominate because of the strong dependence of the radial decay on m.

The magnetic probe is mounted on a pneumatically driven manipulator which may be scanned through a distance of 8 cm in the radial direction within 150 ms. The magnetic probe system on ASDEX then possesses the capability of performing measurements of the radial decay of broadband magnetic fluctuations at a single poloidal location /23/. Previously, other experiments used coils positioned at different poloidal locations around the plasma and inferred the radial decay by plotting the fluctuation amplitude as a function of the radial position of each coil /10,11/. Typically the probe was scanned to within 2 cm of the separatrix. The movement of the probe was restricted to this distance by fears of thermal damage to the probe. Observed perturbations in the hard x-ray flux due to collisions of runaway electrons with the probe were of particular concern.

In Fig. 7, the measurements of the radial decay of the broadband fluctuation amplitude at three frequencies are presented. A number of experimental points are clearly displayed. The dramatic increase in amplitude of the three components as the probe nears the separatrix should be noted. At low frequencies the toroidal component is smaller than the poloidal and radial components, while at higher frequencies they are of comparable magnitude.

Power spectra of the b_r signal at the output of the amplifier in an ohmically heated plasma are shown in Fig. 8. The probe was positioned at various distances from the separatrix. The plasma parameters of the Ohmic discharge were $I_p = 320$ kA, $B_o = 2.17$ T and

$\overline{n_e} = 5.0 \times 10^{19}\ m^{-3}$ (#25278 - 25282). As the distance between the probe and separatrix was increased, the amplitude of the higher frequency components became smaller than the noise level of the amplifier. On JET the frequency spectrum of the probe signal at the output of the amplifier could be limited to 100 kHz because the distance between the probe and separatrix is larger than that on ASDEX /14/. Since 0 dBm corresponds to a signal with an RMS amplitude of 223.6 mV and -20 dBm corresponds to a factor of 10 reduction in signal amplitude, the ratio of b_r/B_θ at $f = 30$ kHz is calculated to be of the order of 10^{-6} when the coils are located 6 cm from the separatrix ($d_s = 4$ cm) in an Ohmic discharge. Magnitudes of the same order are found in other experiments /5, 24/. Assuming an $m = 8$ vacuum decay, a factor of 3 increase in amplitude at the separatrix is estimated. After taking the probe response into account, the frequency dependence of amplitude, A, was found to be $A \propto f^{-\alpha}$ where $\alpha = 2.1 \pm 0.2$.

The power spectrum of broadband magnetic fluctuations for $d_s = 4$ cm in a neutral beam heated plasma and an Ohmic plasma with $I_p = 320$ kA, $B_o = 2.17$ T and $\overline{n_e} = 2.9 \times 10^{19}\ m^{-3}$ (#24022) are compared in Fig. 9. Equilibrium flux surface calculations of the separatrix location show that changes in the fluctuation amplitude cannot be simply explained by a change in the position of the separatrix. The ratio of b_r/B_θ is typically enhanced by a factor of 3 to 5 in neutral beam injection. The ratio is enhanced by a further factor of 3 during ICRH. According to accepted

theoretical calculations /7/, such amplitudes at the separatrix would not be large enough to generate stochastic magnetic field lines and enhance particle and energy transport.

In ASDEX Ohmic discharges, the poloidal component of magnetic field fluctuations contain a coherent fluctuation at f ~ 30 kHz generated by transistor switching noise on the currents in the multipole and vertical field coils. Therefore, although the poloidal component was routinely measured, it was not useful in the study of the radial decay of the magnetic fluctuation amplitude in Ohmic discharges.

The radial decay of the radial and toroidal components of the magnetic field fluctuation amplitude at f = 30 kHz and f = 135 kHz are shown in Fig. 10. The plasma parameters of the Ohmic discharge were $I_p = 320$ kA, $B_o = 2.17$ T and $\overline{n}_e = 5.0 \times 10^{19}$ m^{-3} (#24579). As the probe was scanned to within 2 cm of the separatrix, the coil axis was moved to within 4 cm of the separatrix. The radial decay of the radial and toroidal components is fitted using equation 4.7 and values of m that yield the best fit to the experimental points. As q(a) was varied from 2 to 5, the m value deduced from the radial decay of the radial component varied from 7 to 9. In ASDEX the separatrix is located at r = 40 cm and the metal wall at r = 61 cm.

The possibility that currents were being drawn by the probe and generating the anomalously large toroidal field component was not supported by the experiments in which the graphite cap was alternatively floated and grounded. The measured fluctuation amplitude was identical in each case.

The conjecture that electrostatic coupling could be responsible for the observed signals is invalidated by the consideration that this coupling should be independent of probe orientation. In addition power spectra of density and floating potential fluctuations in ASDEX measured with Langmuir probes show that no appreciable broadband activity occurs at distances greater than 2 cm from the separatrix /25/.

A statistical analysis of the probe signals was undertaken in order to further investigate the possibility that the signals were generated electrostatically. The coherency, γ, was calculated on data sets with 8192 points, digitised at 500 kHz and smoothed over 30 frequency bands /26/. In this case two uncorrelated signals yield $\gamma \approx 0.15 - 0.2$. Statistical analysis of the signals (#21862) show that there was a significant correlation between the poloidal and toroidal components at frequencies up to 100 kHz when the probe to separatrix seperation was 7 cm ($\gamma \approx 0.6$ at 50 kHz). There was a less significant correlation of these two components and the radial component ($\gamma \approx 0.2 - 0.3$ at 50 kHz). There was a high degree of correlation between the outputs of the radially separated coils ($\gamma \approx 0.9$ at all frequencies). This high degree of correlation is consistent with a stochastic source of magnetic fluctuations being located at some distance from the probe. Electrostatic fluctuations would yield a high degree of coherence between the three components.

On TEXT tokamak, a correlation between ion saturation current and magnetic field fluctuations has been observed at large distances

along magnetic field lines /27/. This would suggest that electrostatic waves are guided along magnetic field lines. It has been demonstrated that shear Alfven waves are also guided along magnetic field lines /29/. It is conjectured that the large toroidal component observed in the vicinity of the separatrix could be a feature of this electrostatic wave. The large m values associated with its radial decay tend to support this hypothesis.

In Fig. 11, the radial decay of the fluctuation amplitude in the vicinity of the metal wall of the vacuum chamber is shown. The radial component went to zero at the metal wall as required by theory. The invariance of the amplitude of the poloidal and toroidal field components would indicate that these components are related to the fluctuations in the generated vertical field.

5. SAWTOOTH CRASH INDUCED PERTURBATIONS

The perturbation of the magnetic fluctuation amplitude produced by a sawteeth crash in Ohmic discharges, was observed most clearly when the inversion radius of the sawtooth was largest. The perturbation of the magnetic fluctuation amplitude was also more clearly observed, when the probe to separatrix distance was decreased. For the plasma conditions of $I_p = 460$ kA, $B_o = 1.86$ T and $\overline{n}_e = 2.9 \times 10^{19}$ m^{-3} in these discharges (#25403, 25414, 25417), $q(a) \approx 2$ and the inversion radius is at $r = 28$ cm. The probe was positioned 4 cm from the separatrix. The fluctuations in electron density were simultaneously monitored by a far infrared laser scattering system /30/. The radial position of the scattering volume was altered, so that information concerning the radial variation in frequency spectra was available. All parameters of interest were digitised at 10 kHz.

In Fig. 12, a sawtooth induced perturbation of the electron density and magnetic field fluctuation amplitude is displayed. A density and temperature perturbation initiated by the sawtooth crash propagates towards the separatrix. The perturbation to the electron density and magnetic field fluctuation amplitude are similar when the scattering volume is located at the separatrix. At the high frequency end of the frequency range studied, there exists a response which is simultaneous with the crash of the sawtooth. Over the whole of the frequency range there is also a slower repsonse which is on the time scale of the density and temperature perturbation propagation time to the separatrix. When

the scattering volume was positioned at r = 10 cm or r = 25 cm, the principal feature of the density fluctuation frequency spectrum was a strong peaking in the 10 - 60 kHz frequency band. This is interpreted to be a product of the m = 1 mode associated with the sawtoothing process. Outside the mixing radius this feature is not observed. It is concluded from the simultaniety of the perturbation in magnetic fluctuation amplitude and the edge temperature and density that the source of the magnetic fluctuations for this probe position is located within a few centimetres of the separatrix.

6. PLASMA PARAMETER DEPENDENCE

A systematic study was carried out in a variety of plasma conditions in an effort to identify the underlying physics of the plasma parameter dependence of the broadband magnetic field fluctuations.

6.1 VARIATIONS IN I_p AND B_o

A set of 8 discharges (#25517 - 25525) with a line average density of 2.9×10^{19} m^{-3} and a plasma current of 250 kA, 320 kA or 380 kA in a magnetic field of 1.69 T, 2.17 T, or 2.61 T allowed the amplitude dependence of the magnetic field fluctuations to be studied systematically. The combination of high current and low magnetic field was disruptive because $q(a) \sim 2$.

This series of discharges showed that in the low frequency range the magnetic fluctuation amplitude increased with increasing current at a fixed magnetic field and decreased with increasing magnetic field at a fixed current. This trend suggested that q(a) was the important parameter. In Fig. 13, it may be seen that the magnetic fluctuation amplitude is constant for the set of 3 discharges with the same q(a) and that the magnetic fluctuation amplitude at f = 30 kHz decreases with increasing q(a). At f = 135 kHz a similar, though less severe, dependence of the magnetic fluctuation amplitude on q(a) is observed. At f = 606 kHz the magnetic fluctuation amplitude is even less sensitive to the value of q(a).

The variation of other plasma parameters during this series of discharges is relevant to the identification of the relative importance of each parameter to the measured amplitude. For example,

measurements of the electron density at the separatrix with the lithium beam diagnostic shows that the density scale length varies from 1.5 cm at q(a) = 2 to 2.3 cm at q(a) = 5 /31/. The temperature and density profiles are also dependent on q(a). A distinct flattening of the electron density profile and a less severe broadening of the temperature profile are observed as q(a) is decreased. Because of the small database available, no attempt was made to investigate the scaling of magnetic fluctuation amplitude with changes in all possible plasma parameters.

6.2 VARIATIONS IN $\overline{n}_e$

A set of three discharges (# 24144, 24146, 24148) with $I_p = 380$ kA, $B_o = 2.17$ T and line averaged electron densities of 2.9×10^{19} m^{-3}, 4.3×10^{19} m^{-3} and 5.7×10^{19} m^{-3}, suggests that the magnetic fluctuation amplitude at higher frequencies may be dependent on the line averaged electron density. In Fig. 14, a radial scan of the probe beginning at a distance of 12 cm from the separatrix and moving to within 4 cm of the separatrix shows that at f = 30 kHz and f = 606 kHz the radial profile of the magnetic fluctuation amplitude is insensitive to the line averaged electron density, while at f = 606 kHz a significant difference is observed. The magnetic fluctuation amplitude at this frequency increases with increasing line averaged density. The central value of electron density increases, with no significant broadening or peaking of the profile, as the line averaged density is increased. Similarly, a decrease in central temperature and little change in the profile shape occurs, when the line

averaged density is increased. A systematic increase of power transferred from the separatrix to the divertor with line averaged density is indicated by the intensity of D_α emission in the divertor. This would tend to support a correlation between magnetic fluctuation amplitude and power transfer to the divertor rather than the energy confinement time, since the energy confinement time increases up to densities of 4.3×10^{19} m^{-3} and then saturates as the density is further increased.

Density perturbations induced in a gas oscillation experiment (#24667) demonstrate the dependence of magnetic fluctuation amplitude on gas puffing. The probe was positioned 6 cm from the separatrix and the plasma conditions were $I_p = 320$ kA, $B_o = 2.17$ T and $\overline{n}_e = 2.1 \times 10^{19}$ m^{-3}. In Fig. 15 it is shown that under these conditions an increase in the line averaged electron density resulted in a decrease in the magnetic fluctuation amplitude. This effect is more pronounced at lower densities, as the pertrurbation to the edge plasma conditions induced by the oscillation of the gas puff valve will be more significant at a lower electron density. This observation demonstrates the sensitivity of broadband magnetic fluctuation amplitude to edge plasma parameters.

6.3 IMPROVED OHMIC CONFINEMENT

A new regime with improved energy confinement times in Ohmic plasmas has been found on ASDEX /12/. The improved Ohmic confinement (IOC) regime involves a peaking of the electron density profile when the flow of gas from the puff valve is sharply decreased above a theshold in electron density. Energy confinement times larger than those observed in the saturated Ohmic regime are obtained.

Displayed in Fig. 16 are measurements of the magnetic fluctuation amplitude at various frequencies with the probe positioned at distances of 3 cm and 7 cm from the separatrix. The difference in evolution of the fluctuation amplitude during a transition into the IOC mode is shown. The improvement in energy confinement time is largest for the highest density and the transition occurs soon after the plateau in electron density is reached. Further away from the plasma, the fluctuation level increases as the electron density increases. Of particular significance is the supression of the toroidal field component during the density ramp, where gas puffing is used to raise the electron density. The plasma parameters (#25389 - 25390) were I_p = 420 kA and B_o = 2.36 T and the line averaged electron density was increased in steps with flat top phases at 2.9×10^{19} m^{-3}, 4.3×10^{19} m^{-3} and 5.1×10^{19} m^{-3}.

As shown in Fig. 17, an exceptionally large decrease in fluctuation amplitude was observed when the gas puffing was sharply reduced at time t_2 in another set of discharges (#25344 - 25345). In this

case the probe was also positioned 3 cm from the separatrix. The sharp rise in magnetic fluctuation amplitude marks the transition into the IOC mode and a new equilibrium fluctuation level is reestablished. Although the fluctuation magnitude of the toroidal component is shown in Fig. 17, the same general features were observed when the radial component was studied.

The difference in evolution of magnetic fluctuation amplitude at different probe positions, would suggest that modes with a high poloidal mode number are involved in the IOC transition. At larger distances from the separatrix, the strong radial decay of these modes would mean that a change in the saturated amplitude would be more difficult to observe.

During the sharp transition in D_α, the probe was positioned 3 cm from the separatrix. At this position the probe is positioned 1 cm inside an auxiliary carbon mushroom limiter in its retracted position. It is not clear that the probe is responsible for the unique feature in this IOC transition. In other sets of discharges, no similar sharp transition in D_α occurred when the probe was located 3 cm from the separatrix. Despite the uncertainty in the degree that the probe is influencing the IOC transition, these observations are consistent with the damping of a mode with a large poloidal mode number being involved in the IOC transition.

The energy confinement time and the level of magnetic fluctuations are unrelated in the IOC regime. The magnetic fluctuation amplitude did not vary significantly when the probe was positioned 3 cm from the separatrix, even though the confinement time increased from

80 ms to 130 ms as the density was increased /12/.

The electron temperature and density profiles from the YAG laser were evaluated, in order to establish a link between the change in magnetic fluctuation level and the transition in the plasma parameters. The sequence of events, with respect to the time scale shown in Fig. 17, is as follows. Preceding the abrupt rise in the magnetic fluctuation level, there is a peaking of the electron density. The central density rises and the edge density falls. The electron temperature profile is also gradually evolving during this period, with the temperature rising over the whole of the profile. Then within 20 ms, the magnetic fluctuation amplitude increases by a factor of four. The transition seen on the monitor of D_α in the divertor chamber is simultaneous with the sharp rise in magnetic fluctuation amplitude. After the transition, the central temperature rises further, while the temperature at half radius and at the edge remains constant. The density profile also changes after the transiton. A drop in density at the half radius and a constant density in the centre and edge are observed. Once again, the correlation between D_α intensity in the divertor and the broadband magnetic fluctuation amplitude infer that edge plasma conditions govern the magnitude of magnetic fluctuations and the level of transport into the divertor.

6.4 NEUTRAL BEAM HEATING

A study of the variation of magnetic fluctuation amplitude with neutral beam input power was undertaken in a plasma with $I_p = 380$ kA, $B_o = 2.17$ T and $\overline{n}_e = 2.9 \times 10^{19}$ m^{-3} (#23693). Hydrogen neutrals were injected into a deuterium plasma. The dependence of the magnetic fluctuation amplitude on neutral beam input power is shown in Fig. 18 for three frequencies.

For these discharges, the probe was positioned 5 cm from the separatrix. At f = 30 kHz the measurement reflects the influence of neutral beam heating on the magnitude of the sawteeth and the appearance of coherent Mirnov fluctuations in the frequency range 15 - 25 kHz. This coherent mode has m = 4 or 5 and is driven by the m = 1 mode located in the plasma interior. At higher frequencies the presence of sawteeth may also be seen but the amplitude of the fluctuations are not modulated to the same extent. The increase in magnetic fluctuation amplitude with input power could result from the change in plasma parameter profiles that occur as the neutral beam power is increased. With increasing input power, the central electron temperature increased and the temperature profile was more peaked, while the electron density profile remained independent of input power. The temperature at r = 35 cm increased from 150 eV in the Ohmic discharge to 250 eV with $P_{NI} = 2.5$ MW, while the electron density at this position remained constant at 1.5×10^{19} m^{-3}. The poloidal beta increased from 0.3 in the Ohmic discharge to 0.6 at maximum neutral beam power.

A systematic increase in the intensity of $D\alpha$ emission in the divertor and hence enhanced power flow into the divertor was also noted. These observations support the view that increasing beam power and enhanced broadband magnetic fluctuation amplitude are correlated with the deterioration of the energy confinement time. However, this simple view overlooks the changes in edge plasma parameters that are produced as neutral beam power is increased.

In Fig. 19 the amplitude dependence of the broadband magnetic fluctuations on the direction of neutral beam injection with repect to the plasma current is displayed. In each case the target plasma, with $I_p = 420$ kA, $B_o = 2.0$ T, $\overline{n}_e = 5.0 \times 10^{19}$ m^{-3} and 0.94 MW of D^o injection into a deuterium plasma (#25711 - 25726), was identical. Apart from the effects of sawtooth stabilisation in those discharges with counter injection, the radial component of magnetic fluctuations at f = 135 kHz and f = 606 kHz shortly after the beginning of neutral injection show no sensitivity to the change in direction of neutral beam injection. In both discharges the energy confinement time was approximately 55 ms at this time. At later times the energy confinement time is larger in discharges with counter injection /32/. The rise in electron density during the counter injection discharge could be the reason for the differences in magnitude observed at the end of the time scale shown. Hence, it is not clear whether a cause and effect relationship can be claimed between the decrease in amplitude of magnetic fluctuations and the increase in confinement time.

6.5 H – MODE

In Fig. 20 the magnetic fluctuation amplitude in discharges with the same nominal conditions of $I_p = 380$ kA, $B_o = 2.17$ T and $\bar{n}_e = 2.9 \times 10^{19}$ m^{-3} with 2.6 MW of H° injection into deuterium (#24895 - 24896) are shown. The upper traces correspond to the discharge which remained in the L-mode and the lower traces correspond to the discharge which made a transition into the H - mode. The transition into the H - mode is coincident wtih the formation of a steep density gradient and a temperature pedestal in the vicinity of the separatrix.

This dramatic change in edge plasma parameters is coincident with a dramatic change in the magnetic fluctuation amplitude. The coherent magnetic fluctuations and the incoherent fluctuations are of smaller amplitude in the discharge during the H - mode. Fig. 21 clearly displays that the transition to the H - mode was followed by an increase in the coherent magnetic fluctuation amplitude and a sharp decrease in activity at f = 82 kHz. This difference in behaviour suggests that the mechanism reponsible for the generation of coherent fluctuations (an m = 4 mode) is not directly linked to the instability generating the fluctuations at a slightly higher frequency. Further investigations are required to determine whether or not the stabilisation of fluctuations in the low frequency range are the cause or a product of the transition into the H - mode. It is also evident from the increase in amplitude of the b_z component at high frequencies after the transition that a different mode has been destabilised. In the discharge which remains in the L - mode

the toroidal component remains at a similar amplitude as that displayed in Fig. 21 prior to the H - mode transition. It is suggested that these fluctuations are related to the high m modes observed in Ohmic discharges. Preliminary observations of the amplitude variation of the toroidal component with the probe positioned 4 cm from the separatrix show that the amplitude may increase by more than a factor of 10 during the H - mode. It is also noteworthy that the activity at high frequencies in the radial component before the transition has no counterpart in the toroidal component.

A powerful demonstration of the independence of the response of each channel of the frequency comb may be seen in Fig. 22. The time evolution of the amplitude of each frequency component is clearly related to the sawtooth crashes.

6.6 ISOTOPE DEPENDENCE

The amplitude dependence of the magnetic fluctuations at f = 135 kHz and f = 606 kHz in a plasma with either hydrogen or deuterium as the filling gas is plotted in Fig. 23. The plasma conditions were I_p = 380 kA, B_o = 2.36 T and $\overline{n_e}$ = 4.2 x 10^{19} m^{-3} with 1.3 MW (4 sources) of H^o injection (#25757 - 25771). Only the radial dependence of the magnetic fluctuation amplitude during neutral beam injection is shown, as no significant differences were observed in the Ohmic stage of the discharge. An appreciable difference in amplitude exists only when the probe is located close to the separatrix. The observation that broadband magnetic fluctuations increase when deuterium is used in the place of

hydrogen, is not consistent with the conjecture of a link between energy confinement time and fluctuation amplitude, since the energy confinement time increases with the change in working gas. It should be noted, that similar increases in the amplitude of broadband electron density fluctuations after a change in working gas were also observed on ASDEX /29/. The higher gas puffing rate necessary to maintain a constant line averaged density in the hydrogen discharge is suggested as the reason for the difference in magnetic fluctuation amplitude in the two discharges /33/.

6.7 ION CYCLOTRON RESONANCE HEATING

The dependence of magnetic fluctuation amplitude on ICRH (#25262, P_{ICRH} = 1.7 MW) with the probe positioned 2 cm from the separatrix is shown in Fig. 24. The dependence of magnetic fluctuation amplitude on ICRH (#25234, P_{ICRH} = 1.5 MW) with the probe positioned 10 cm from the separatrix is shown in Fig. 25. In both discharges the plasma parameters were I_p = 380 kA, B_o = 2.36 T and the neutral beam input power was 1.25 MW. The difference in evolution of the electron density in these discharges was due to changes in the impurity level. Different levels of impurities on these different days would cause the observed difference in behaviour.

At f = 30 kHz the influence of ICRH on sawtooth amplitude was identified as the principle link between magnetic fluctuation amplitude and input power. Coherent Mirnov activity at 15 - 25 kHz is commonly observed in plasmas with ICRH, and the measured amplitude in the

lower frequency channels is thus dominated by the magnitude of the coherent magnetic fluctuatiions. At higher frequencies it was observed that the magnetic fluctuation amplitude depended on input power when the probe was located 10 cm from the separatrix, and the magnetic fluctuation amplitude saturated with input powers greater than 1 MW. The measured amplitude in the higher frequency channels is independent of sawteeth activity.

When the probe was moved away from the separatrix, a factor of 6 increase of the amplifier gain was required and the relative amplitude of the higher frequency magnetic fluctuations with neutral injection alone and with neutral injection plus ICRH changed. These observations suggests that the m number of the high frequency fluctuations was strongly reduced by ICRH. In the vicinity of the separatrix the saturated amplitude of the magnetic fluctuations was not strongly altered.

A scan of B_o for constant ICRH input power showed the influence of the power deposition radius on the magnetic fluctuation amplitude. A minimum in magnetic fluctuation amplitude was observed when the power deposition radius was coincident with the plasma centre. A distinct increase in magnetic fluctuation amplitude was observed as the power deposition radius moved towards the outer edge of the plasma. A corresponding but less severe increase was also oberved as the power deposition radius moved towards the inner edge of the plasma.

7. CONCLUSIONS

The relationship between the parameters of the edge plasma and the magnitude of the broadband magnetic fluctuation amplitude has been demonstrated. The reaction of the magnetic fluctuation amplitude to the changes in edge plasma parameters induced by a sawtooth crash or by gas puffing shows this most clearly.

The link between the power transferred into the divertor, as measured by the intensity of D_α emission in the divertor, and the amplitude of magnetic fluctuations is clearly displayed in all the discharge regimes of ASDEX. In the density dependence of magnetic fluctuations in Ohmic discharges, in the IOC mode, in the neutral beam power dependence of magnetic fluctuations and in the H-mode a correlation between the intensity of D_α emission in the divertor and the amplitude of magnetic fluctuations was observed.

The hypothesis of a link between the global energy confinement time and the broadband magnetic fluctuation amplitude was not supported. In those experiments with neutral beam injection, the power dependence of the magnetic fluctuation amplitude and the reduction in magnetic fluctuation amplitude in counter injection discharges corresponded to the predicted change in energy confinement time. However, in other discharge regimes this hypothesis is clearly contradicted. An increase in fluctuation amplitude and an improvement in confinement time were simultaneously observed when the probe was positioned close to the separatrix and when the working gas was

changed from hydrogen to deuterium. In addition, the improvement in confinement time in the IOC regime was not reflected in a corresponding decrease in the magnetic fluctuation amplitude.

Theoretically, values of poloidal beta below one infer that electromagnetic wave instabilities will not be strongly excited. Experimentally, the small amplitude of the magnetic fluctuations, the sawtooth induced perturbation of the magnetic fluctuation amplitude, the existence of the toroidal component in the vicinity of the separatrix with an m number of 25 and the experimental results from TEXT suggest that the source of the observed broadband magnetic fluctuations on ASDEX is the magnetic component of an electrostatic wave instability that is located within a few centimetres of the separatrix. The connection between good confinement, as monitored by D_α emission in the divertor, and magnetic fluctuation amplitude shows that these electrostatic instabilities in the edge plasma are playing the dominant role in determining the quality of confinement.

8. REFERENCES

/1/ P.C. Liewer,
Nucl. Fusion, 25, 543, 1985.

/2/ C.P. Ritz, R.D. Bengston, S.J. Levinson and E.J. Powers,
Phys. Fluids, 27, 2956, 1984.

/3/ C. Hollenstein et al.,
CRPP Report, LRP 306, 1986.

/4/ M. Malacarne and P.A. Dupperex,
JET Report, JET-P (87) 26.

/5/ K. McGuire et al.,
PPPL Report, PPPL 2435, 1987.

/6/ W.M. Tang,
Nucl. Fusion, 18, 1089, 1978.

/7/ A.B Rechester and M.N. Rosenbluth,
Phys. Rev. Lett, 40, 38, 1978.

/8/ P.H. Diamond, P.L. Similon, T.C. Hender, and B.A. Carreras,
University of Texas Report, IFSR 113, 1983.

/9/ B.A. Carreras et al.,
Phys. Rev. Lett., 50, 503,1983.

/10/ N. Ohyabu et al.,
Phys. Rev. Lett., 58, 120, 1987.

/11/ M. Malacarne et al.,
JET Report, JET-P (87) 22.

/12/ F. Söldner et al.,
Phys. Rev. Lett., 61, 1105, 1988.

/13/ A.B. Mikhailovskii,
"Reviews of Plasma Physics" (M.A. Leontovich , Ed.),
Vol. 3., 159, 1967.

/14/ B.B Kadomstev,
"Plasma Turbulence", p. 79.
(Academic Press, London, 1965)

/15/ N.A. Krall and A.W. Trivelpiece,
"Principles of Plasma Physics", p. 206.
(McGraw-Hill, New York, 1973)

/16/ N.G. Van Kampen and B.U. Felderhof,
"Theoretical Methods in Plasma Physics, p. 62.
(North Holland, Amsterdam, 1967)

/17/ E.D. Fredrickson and P.M. Ballan,
Phys. Fluids, 28, 1866, 1985.

/18/ R.E. Waltz,
Phys. Fluids, 28, 577, 1985.

/19/ N.T. Gladd, J.F. Drake, C.L. Chang, and C.S. Liu
Phys. Fluids, 23, 1182, 1980.

/20/ G.S. Lee and P.H. Diamond,
Phys. Fluids, 29, 3291, 1985.

/21/ A.J. Wooton, S.C. Bates and C.E. Bush,
Oak Ridge National Laboratory Report, TM - 8648, 1983.

/22/ G.Bateman,
"MHD Instabilities", p. 111.
(MIT Press, New York, 1978)

/23/ F. Ryter, A. Pochelon, and F. Hoffmann,
14 th European Conference on Controlled Fusion
and Plasma Physics, (Madrid), Vol. I, 265, 1987.

/24/ F. Crisanti, M. Marinucci and C. Nardone,
16th European Conference on Controlled Fusion
and Plasma Physics, (Venice), Vol. I, p. 139, 1989.

/25/ A. Rudyj et al.,
16th European Conference on Controlled Fusion
and Plasma Physics, (Venice), Vol. I, p. 27, 1989.

/26/ D.E. Smith, E.J. Powers and G.S. Caldwell,
IEEE Transactions on plasma science, Vol. 2, p. 261, 1974.

/27/ Y. J. Kim et al.,
Nucl. Fusion, 29, 99, 1989.

/28/ A.I. Zverev,
"Handbook of Filter Synthesis"
(John Wiley and Sons, New York, 1967)

/29/ G. G. Borg et al.,
Plasma Physics and Cont. Fusion, 27, 1125, 1985

/30/ G. Dodel and E. Holzhauer,
15th European Conference on Controlled Fusion
and Plasma Heating, (Dubrovnik), Vol. I, p. 43, 1988.

/31/ K. McCormick,
private communication.

/32/ O. Gehre et al.,
Phys. Rev. Lett., 60, 1502 1988.

/33/ E. Holzhauer,
private communication.

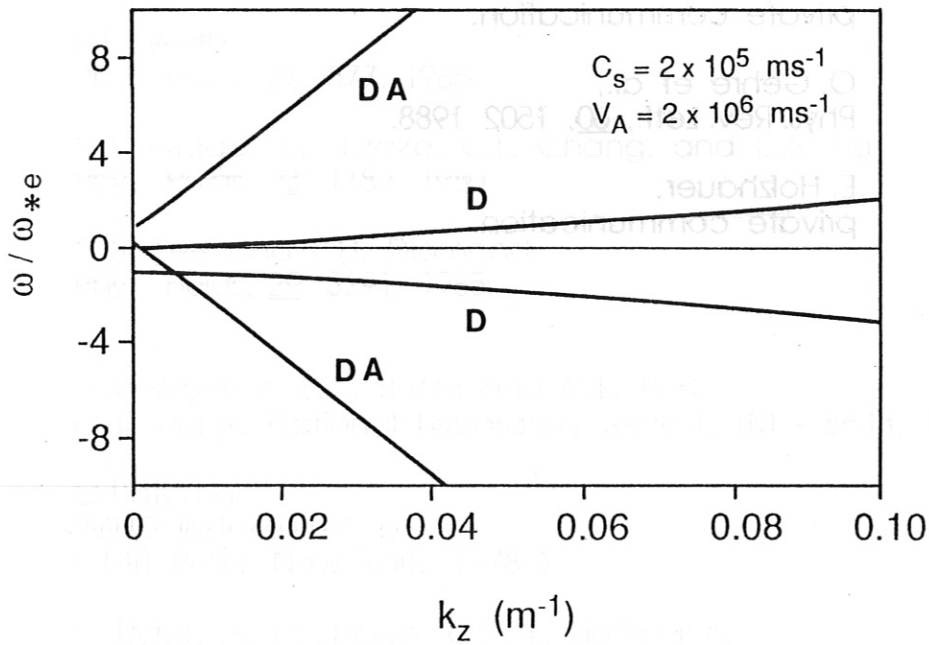

Fig. 1 Dispersion relations for the drift wave (D) and drift - Alfven (DA) wave in an inhomogeneous plasma.

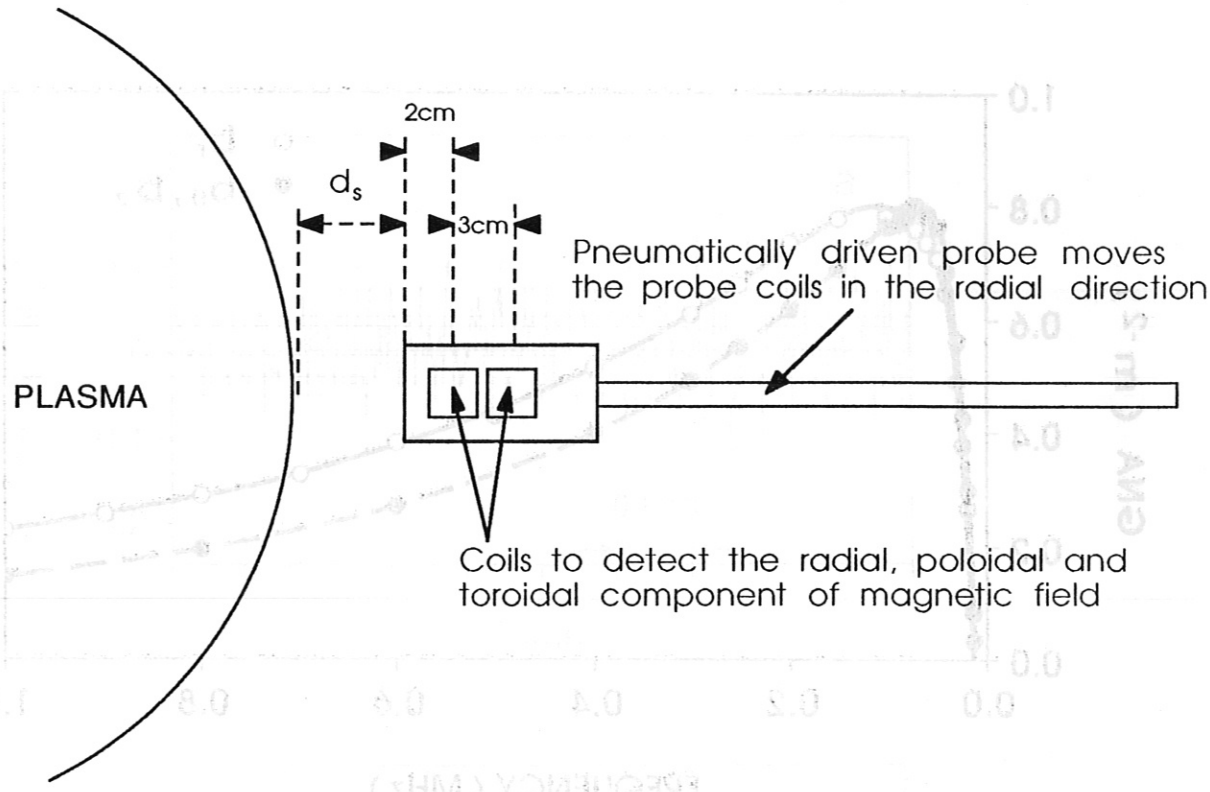

Fig. 2 A schematic diagram of the experimental apparatus. The distance, d_s, between the probe surface and the plasma separatrix is defined. The axes of the first set of coils are 2.0 cm from the probe surface facing the plasma and the separation of the axes of the two sets of coils is 3.0 cm.

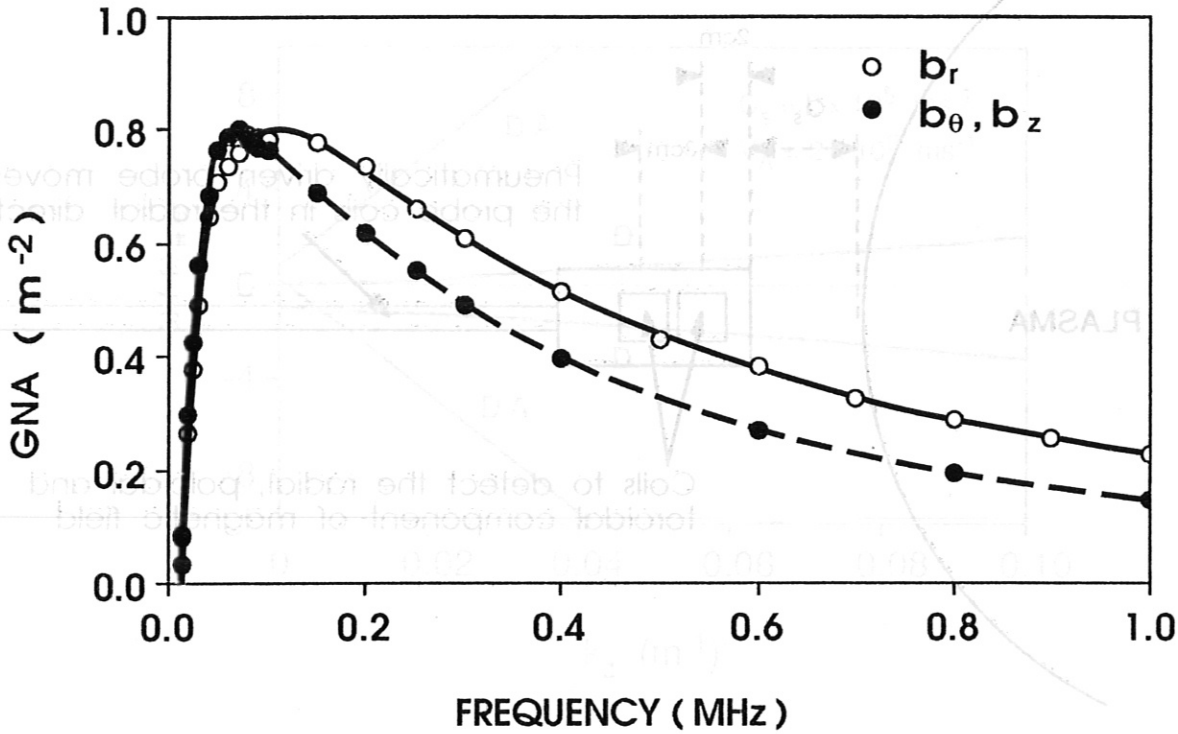

Fig. 3 The calibration curves of the system for each of the different orientations of the coils when connected to the high pass filter and the amplifier set to a gain of 100.

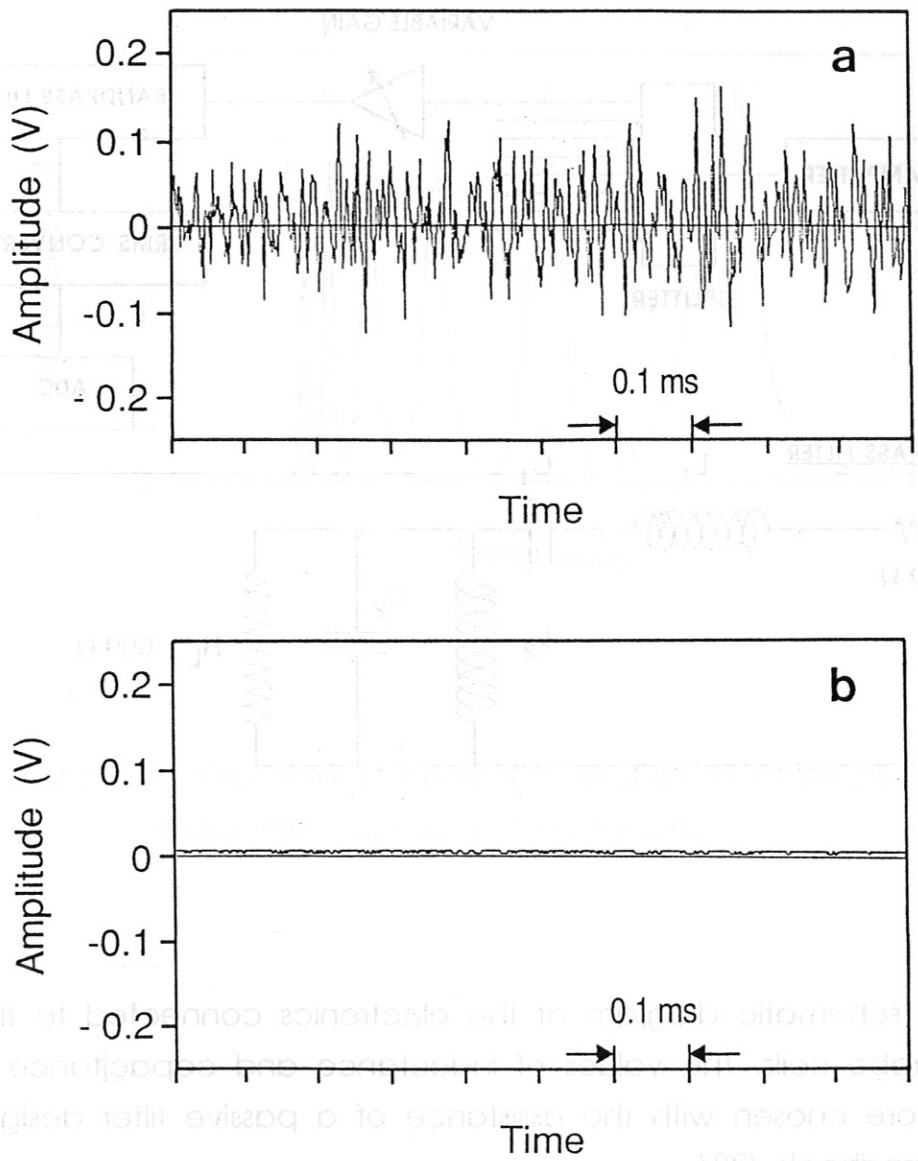

Fig. 4 A typical output signal at the amplifier in an Ohmic discharge. The noise signal was obtained in a second discharge by withdrawing the probe the maximum distance (50 cm) from the plasma.

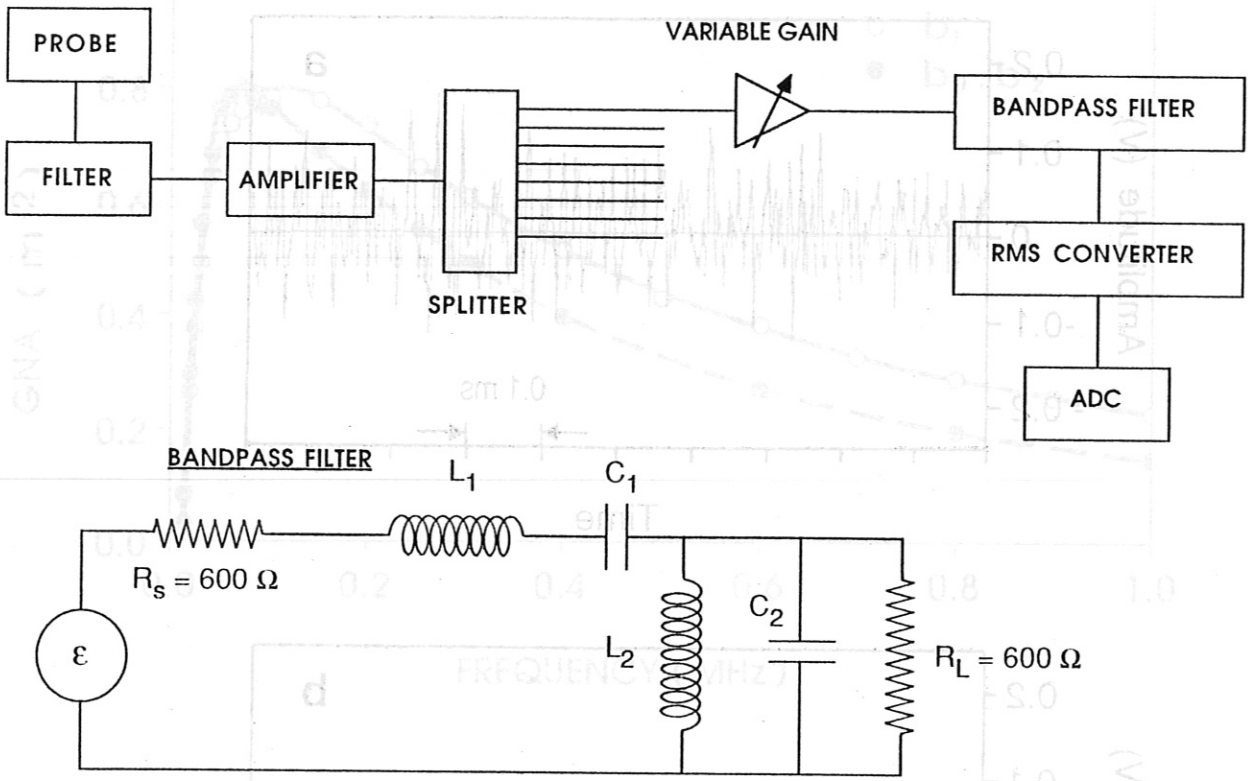

Fig. 5 A schematic diagram of the electronics connected to the probe coils. The values of inductance and capacitance were chosen with the assistance of a passive filter design handbook /28/.

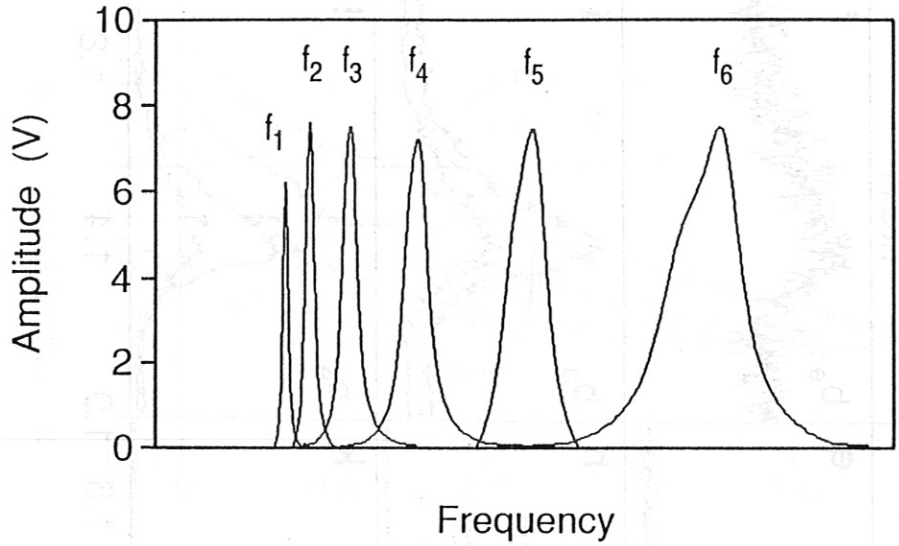

Fig. 6 A sinusoidal input to the frequency comb, swept in frequency, yields the reponse curves shown.

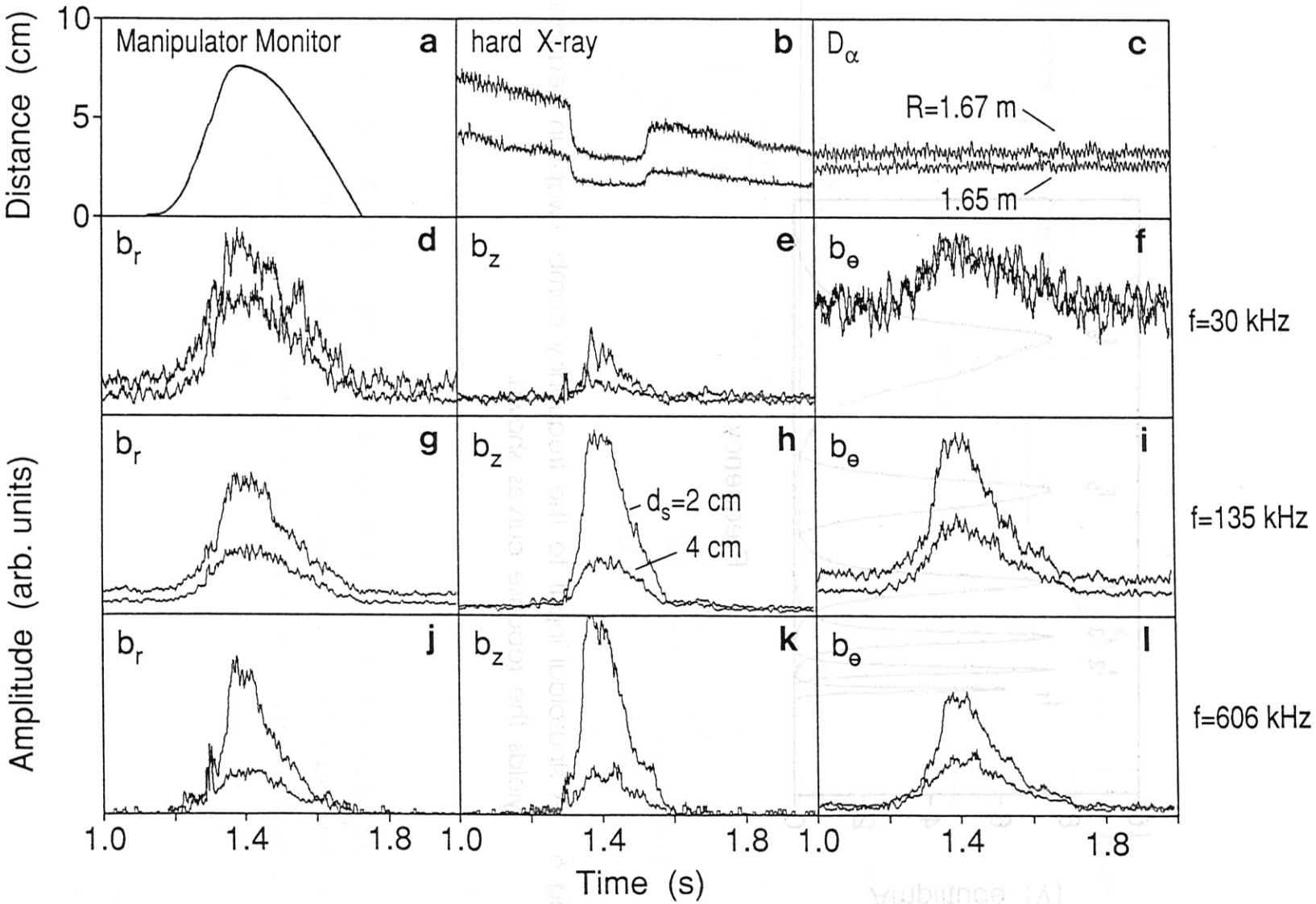

Fig. 7 Radial scans of the radial, toroidal, and poloidal fluctuation amplitude measured by the frequency comb. Two radial scans are shown, with $d_s = 2$ cm and $d_s = 4$ cm.

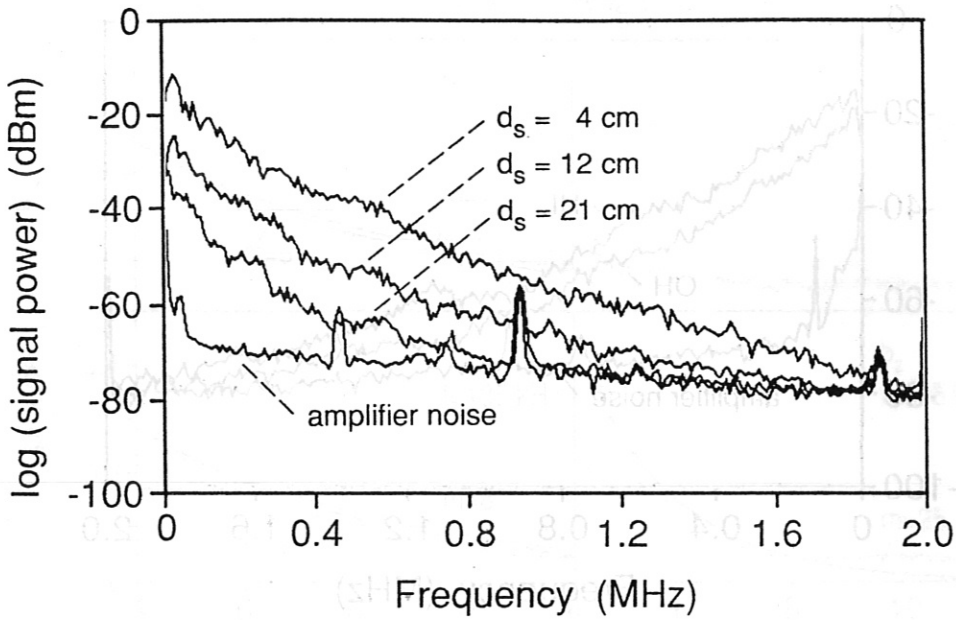

Fig. 8 Power spectra of the b_r component as a function of the probe distance to the separatrix in ohmic discharges.

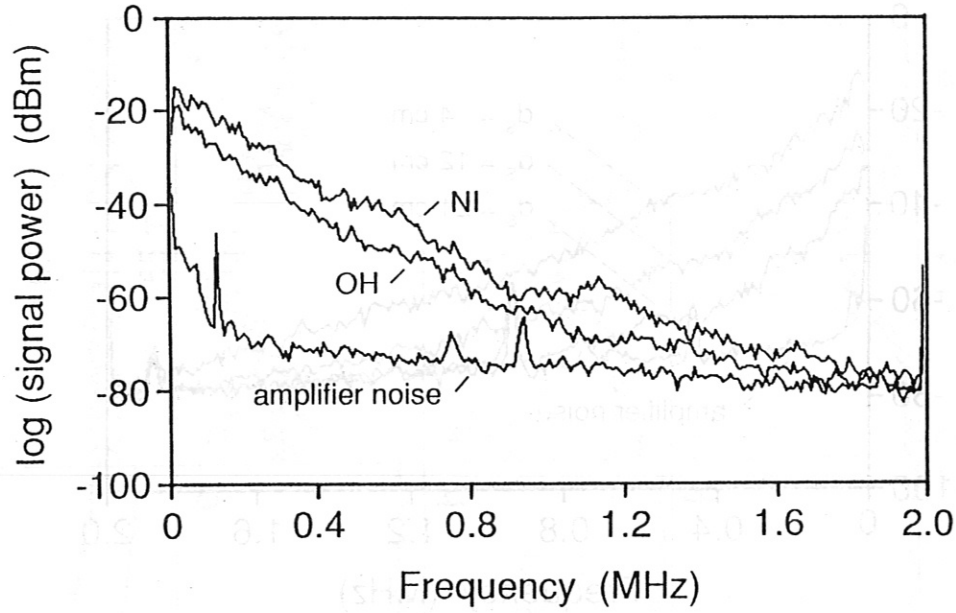

Fig. 9 Power spectra of the b_r component showing the enhancement of the broadband magnetic fluctuation amplitude with neutral beam injection.

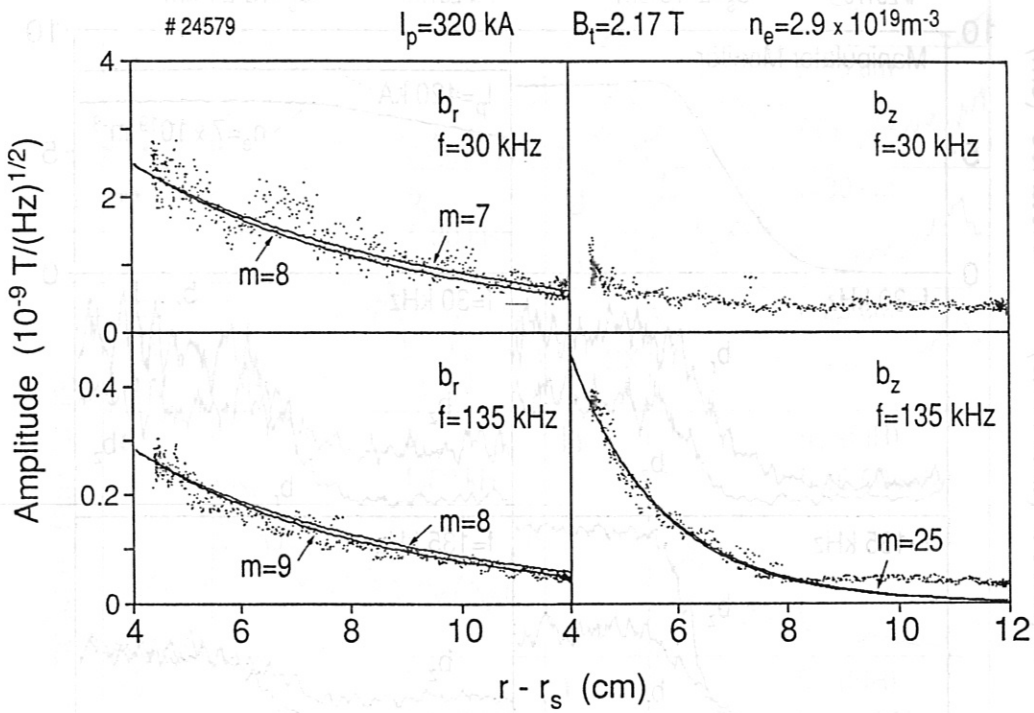

Fig. 10 The radial decay of the b_r and b_z component at f = 30 kHz and at f = 135 kHz versus distance to the separartrix, r - r_s.

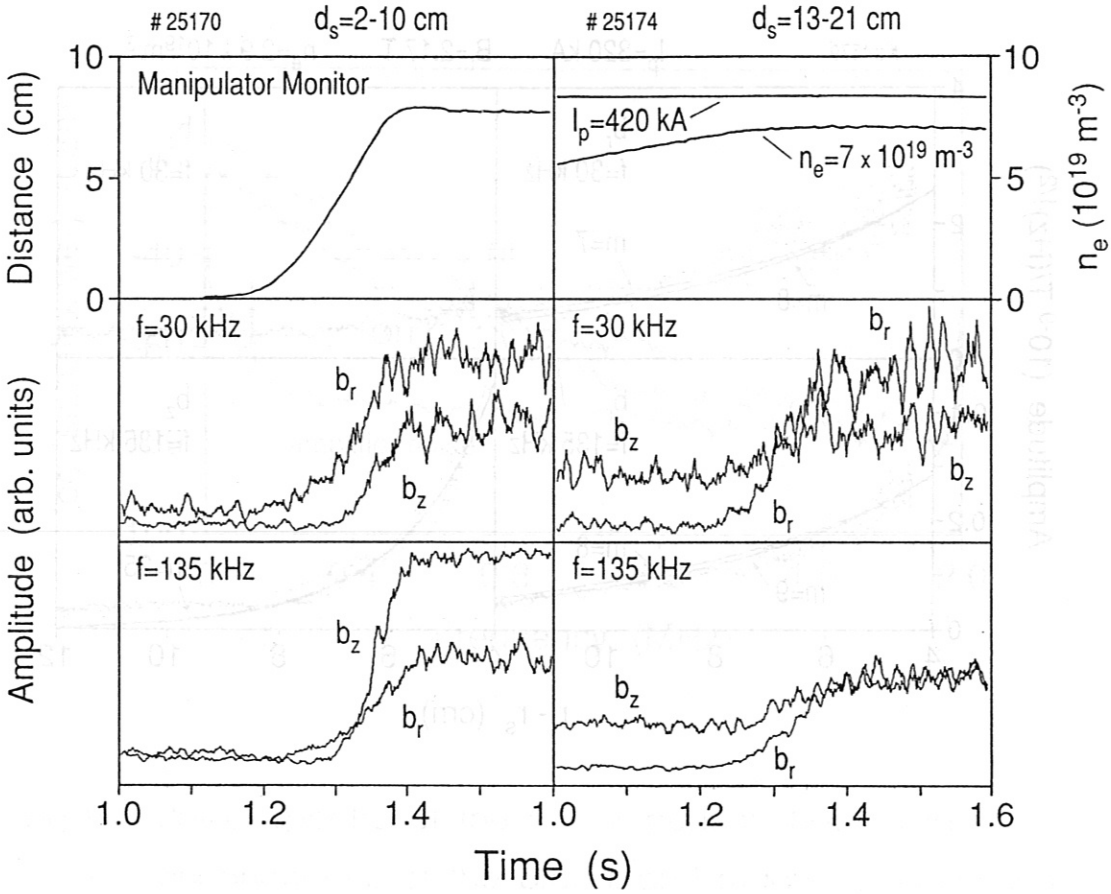

Fig. 11 The radial decay of the b_r and b_z component at f = 30 kHz and f = 135 kHz in the vicinity of the metal wall of the vacuum chamber.

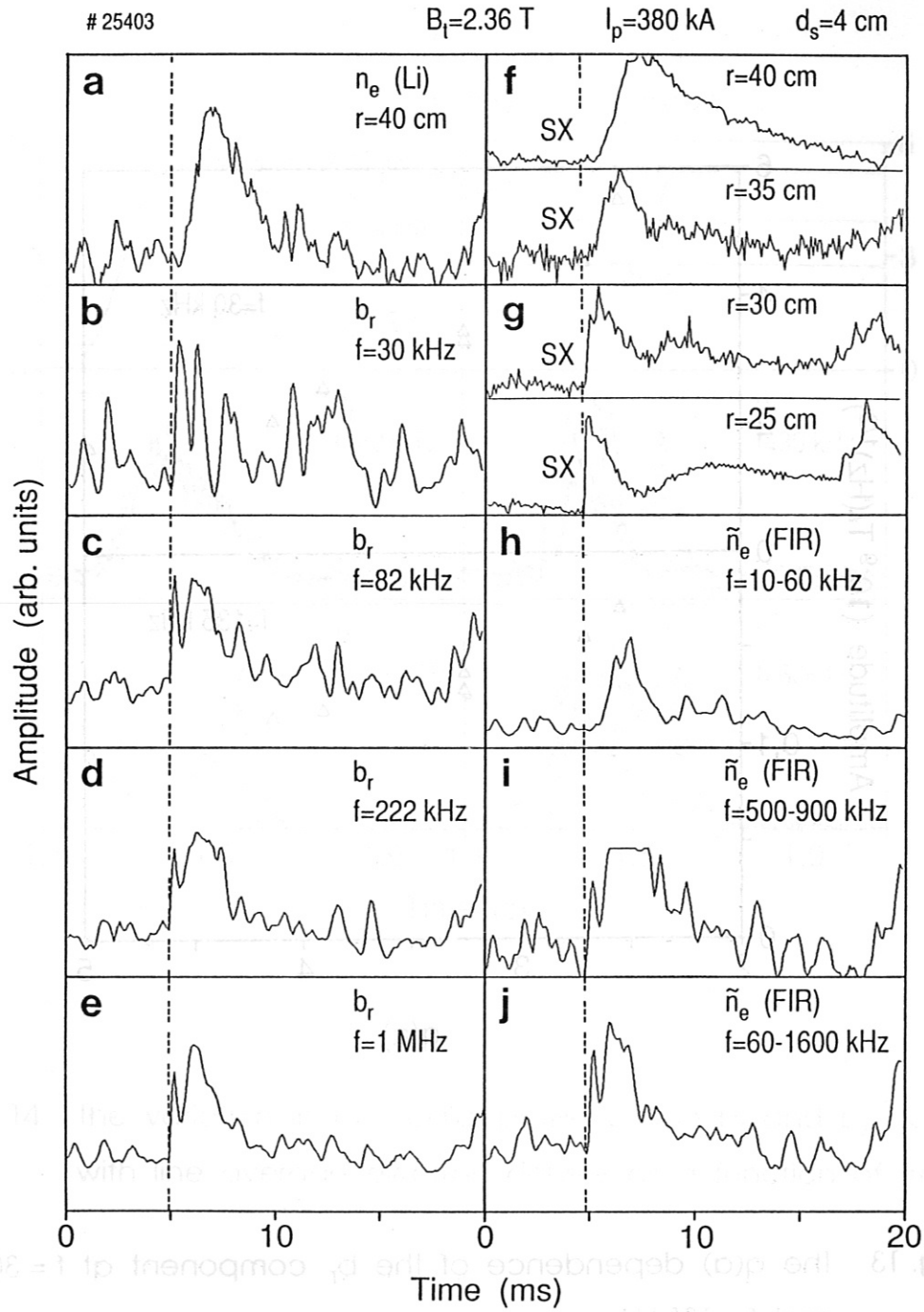

Fig. 12 Perturbations of the magnetic field and electron density fluctuation amplitude associated with sawtooth induced perturbations of the plasma.

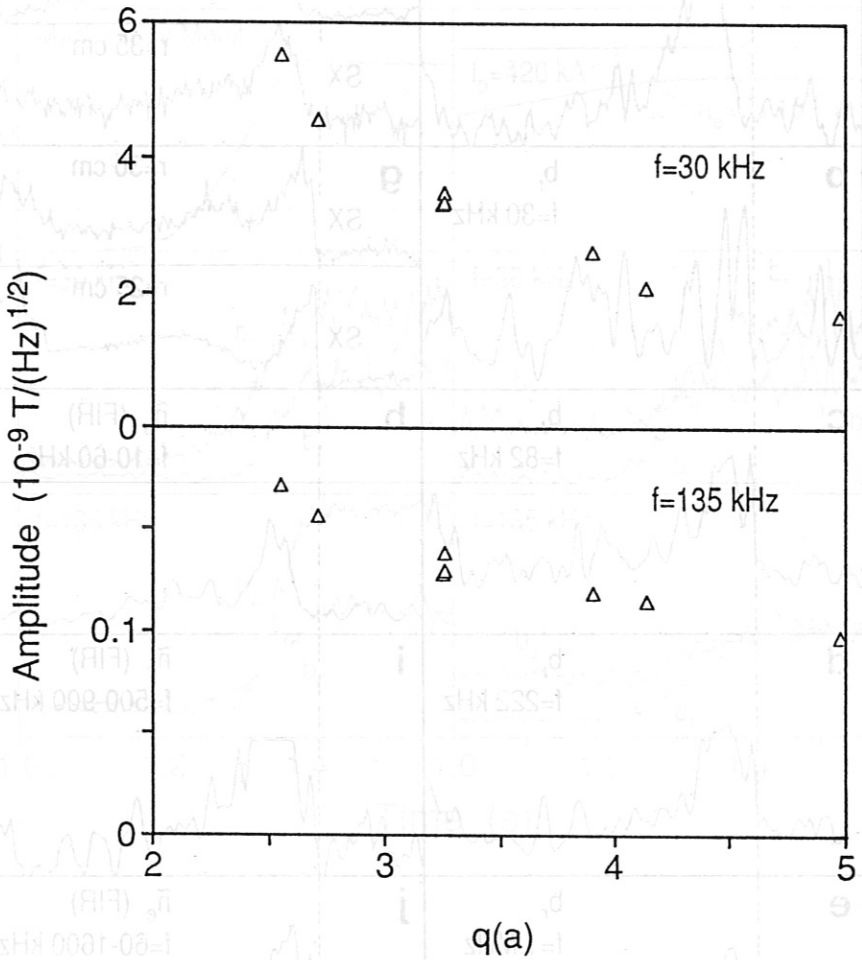

Fig. 13 The q(a) dependence of the b_r component at f = 30 kHz and f = 135 kHz.

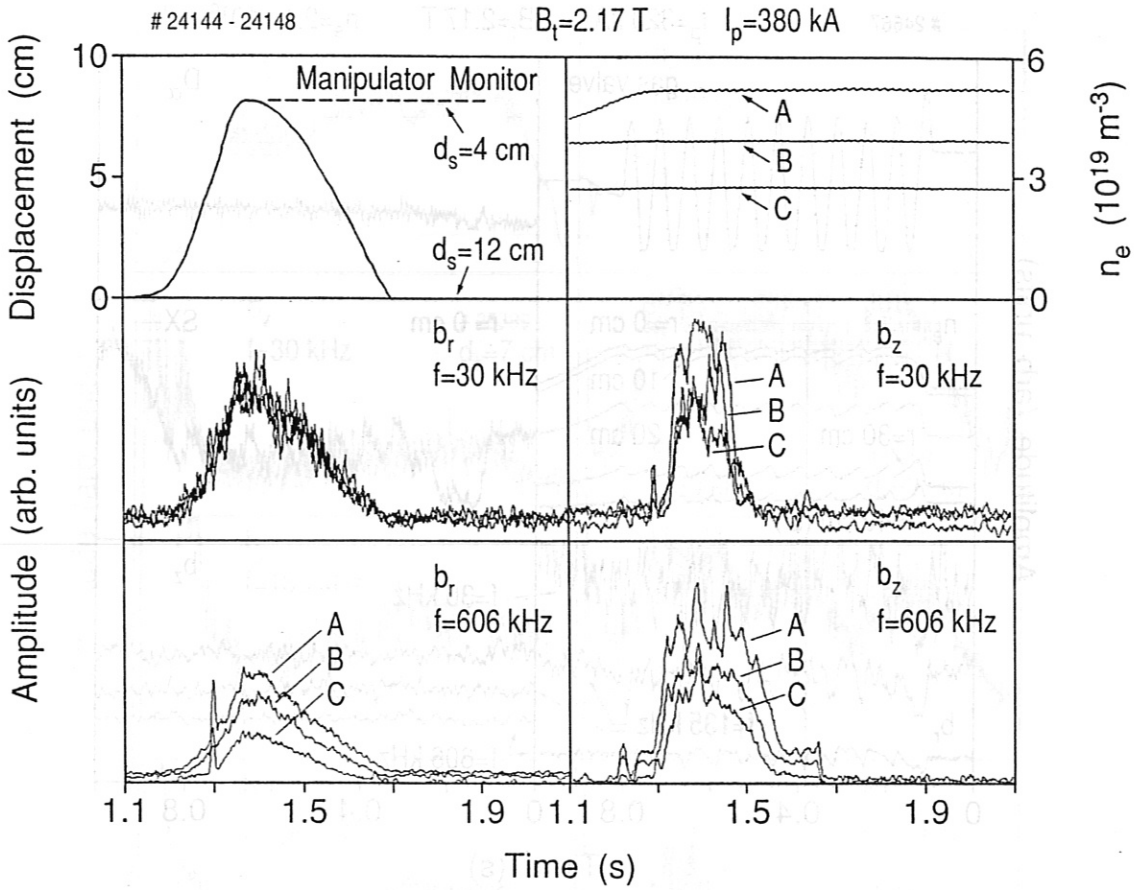

Fig. 14 The variation in the radial profile of the b_r and b_z component with line average electron density as a function of frequency.

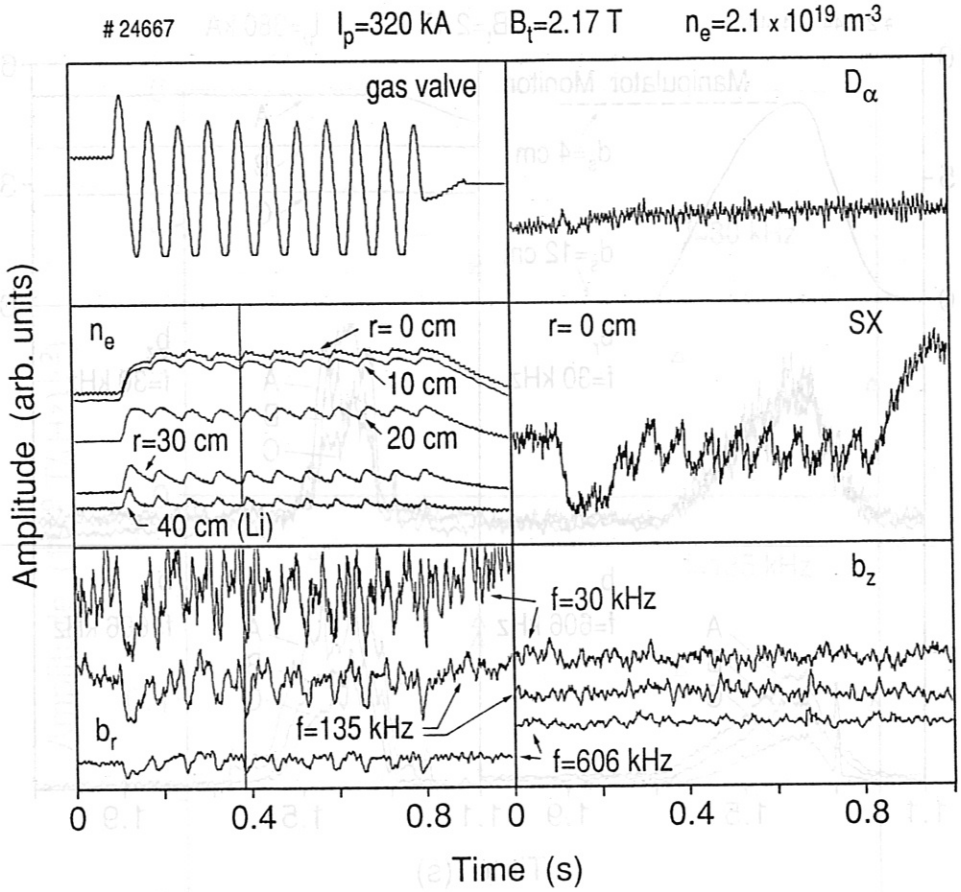

Fig. 15 The correlation of gas puff oscillations and the perturbation of the broadband magnetic fluctuation amplitude.

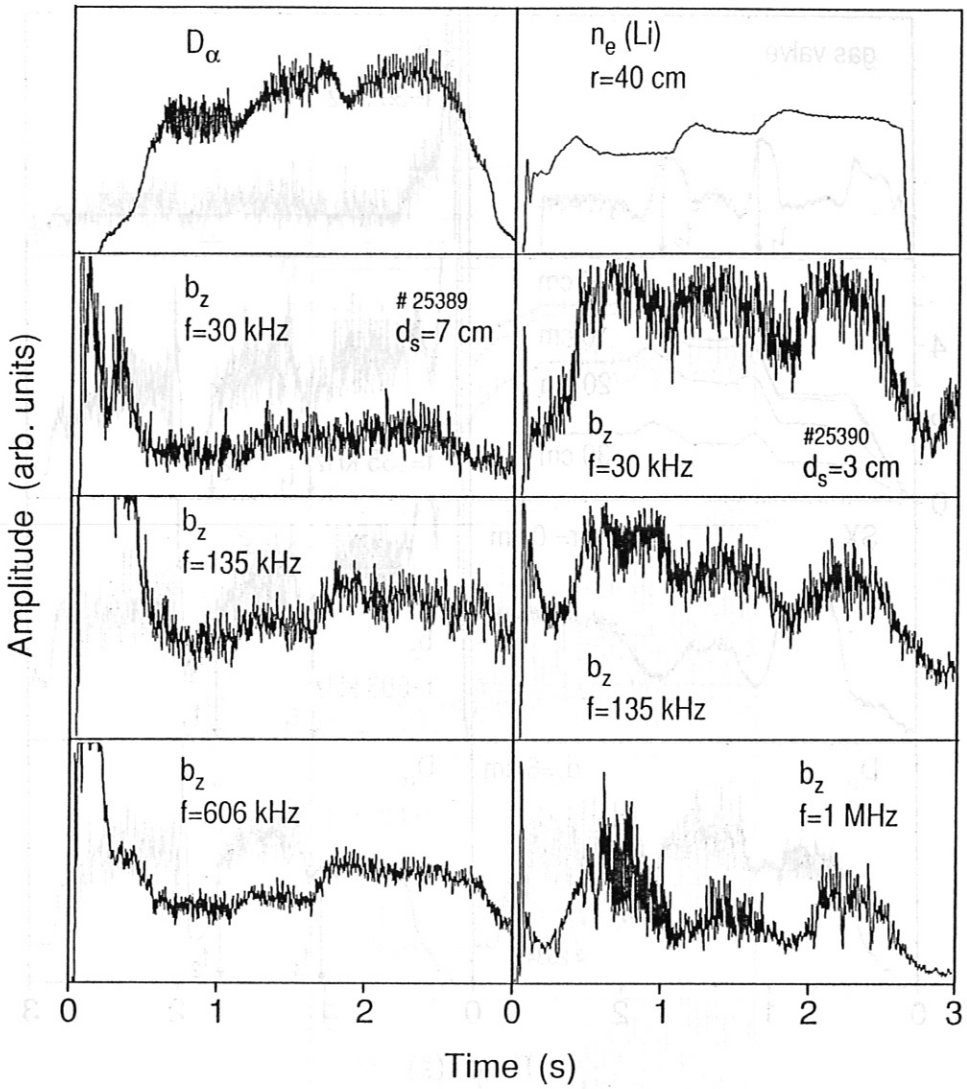

Fig. 16 Radial dependence of broadband magnetic fluctuation amplitude during an IOC transition.

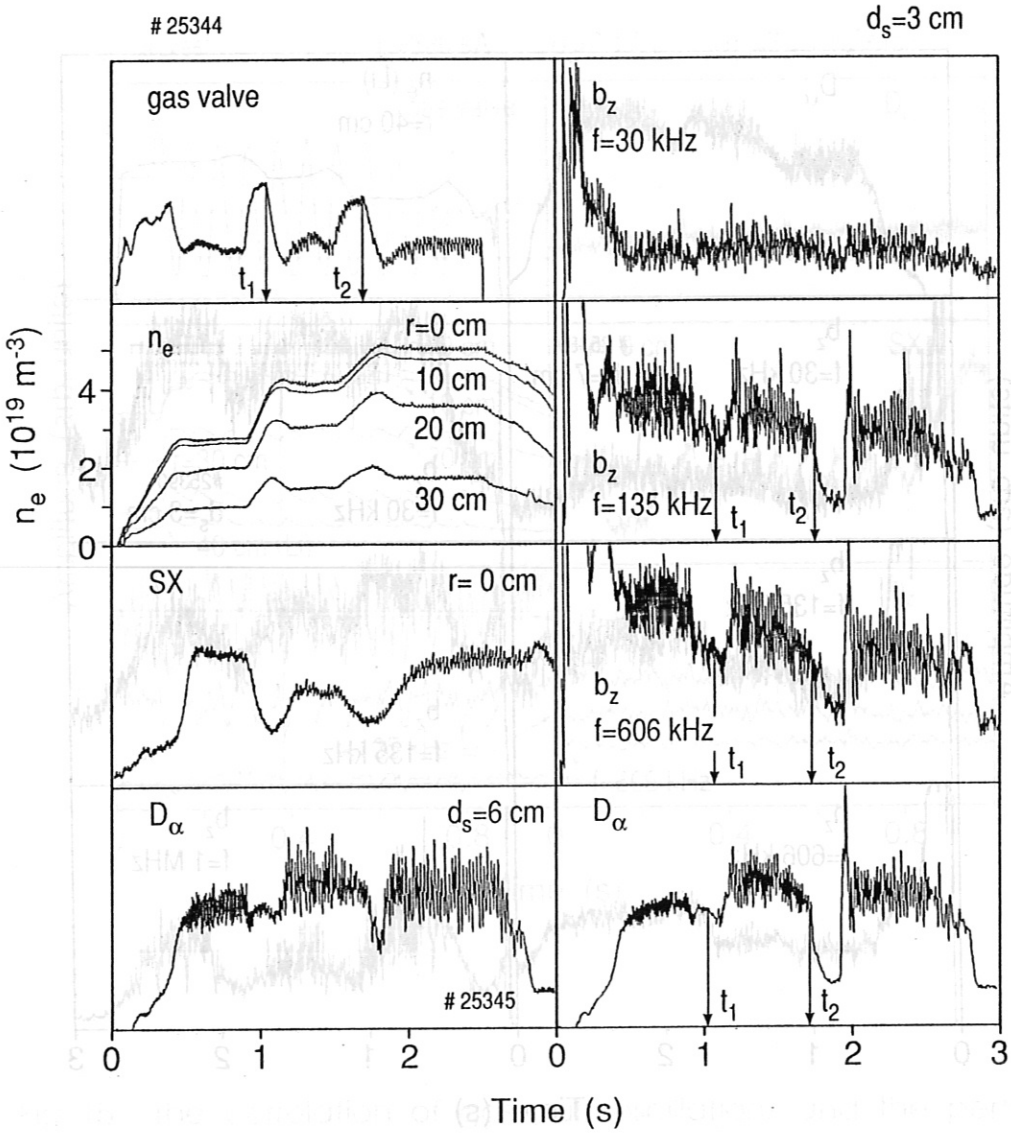

Fig. 17 Correlation of D_α emission in the divertor with broadband magnetic fluctuation amplitude during an IOC discharge.

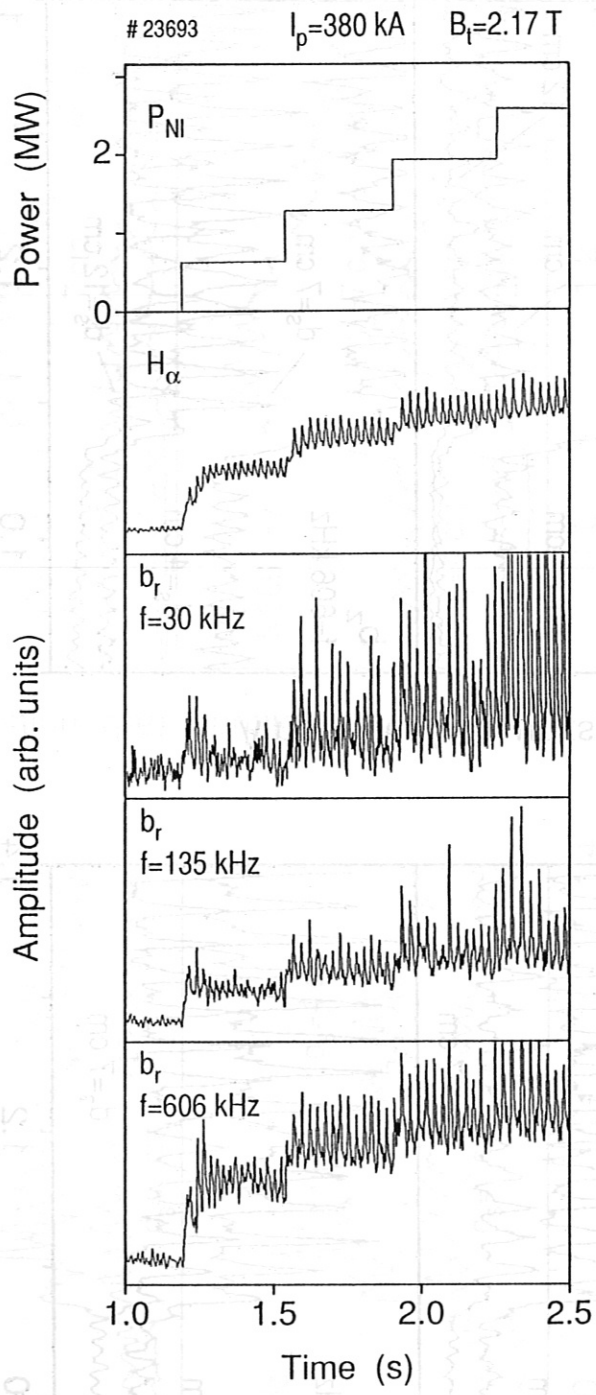

Fig. 18 The dependence of broadband magnetic fluctuation amplitude on neutral beam input power.

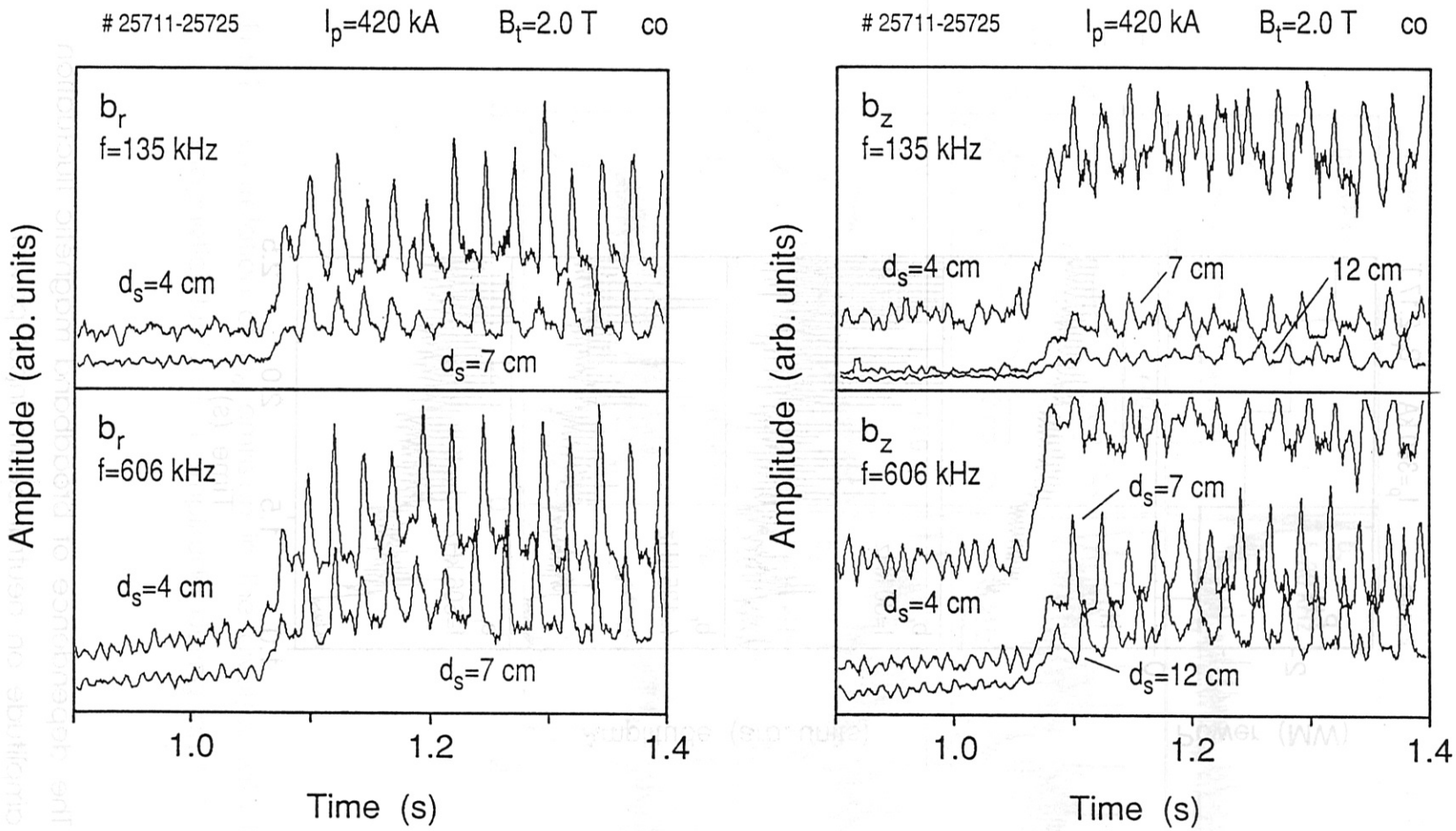

Fig. 19 (a) Broadband magnetic fluctuations in plasmas with co-injection of neutral beams.

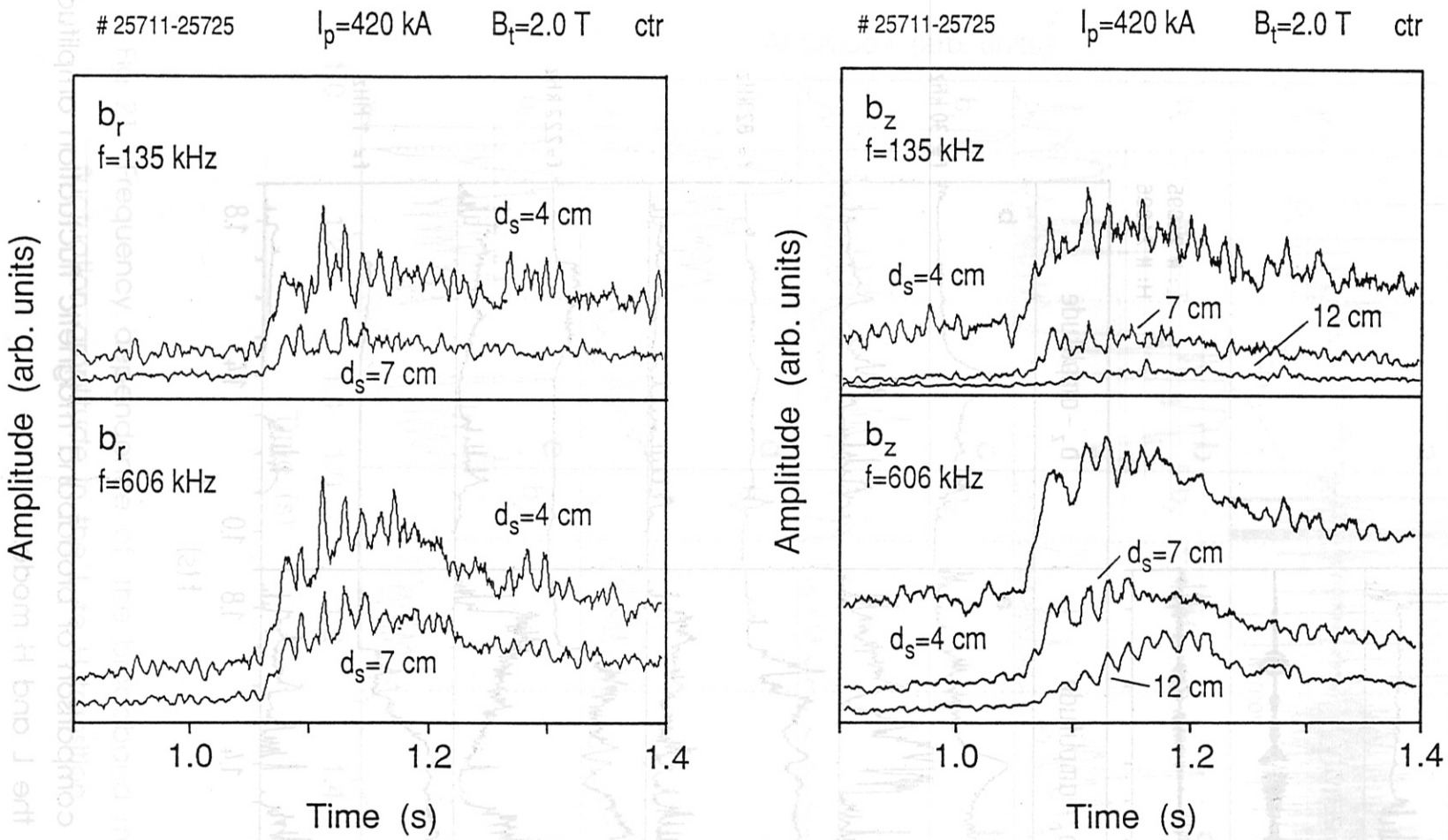

Fig. 19 (b) Broadband magnetic fluctuations in plasmas with counter injection of neutral beams.

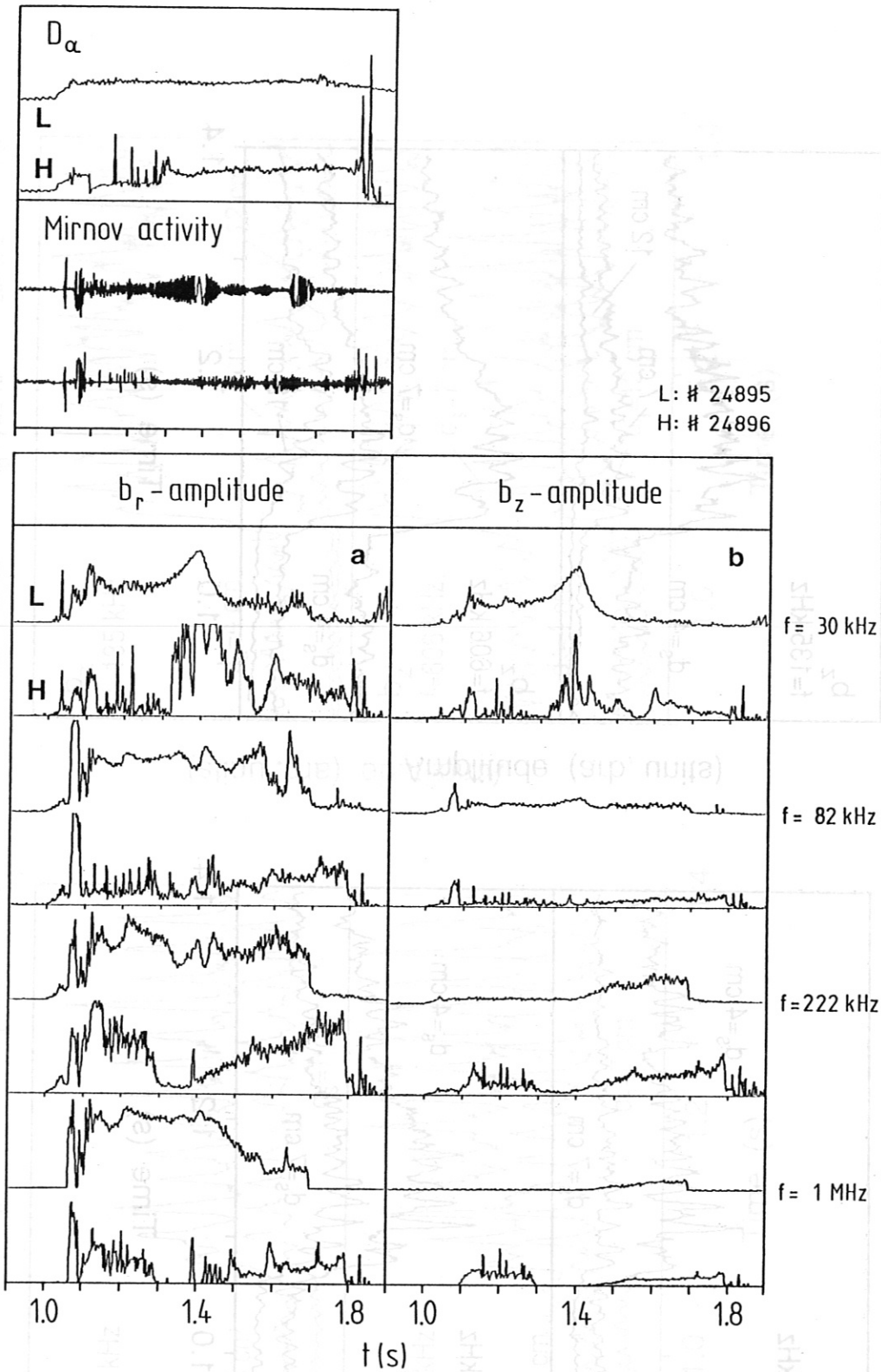

Fig. 20 A comparison of broadband magnetic fluctuation amplitude in the L and H mode.

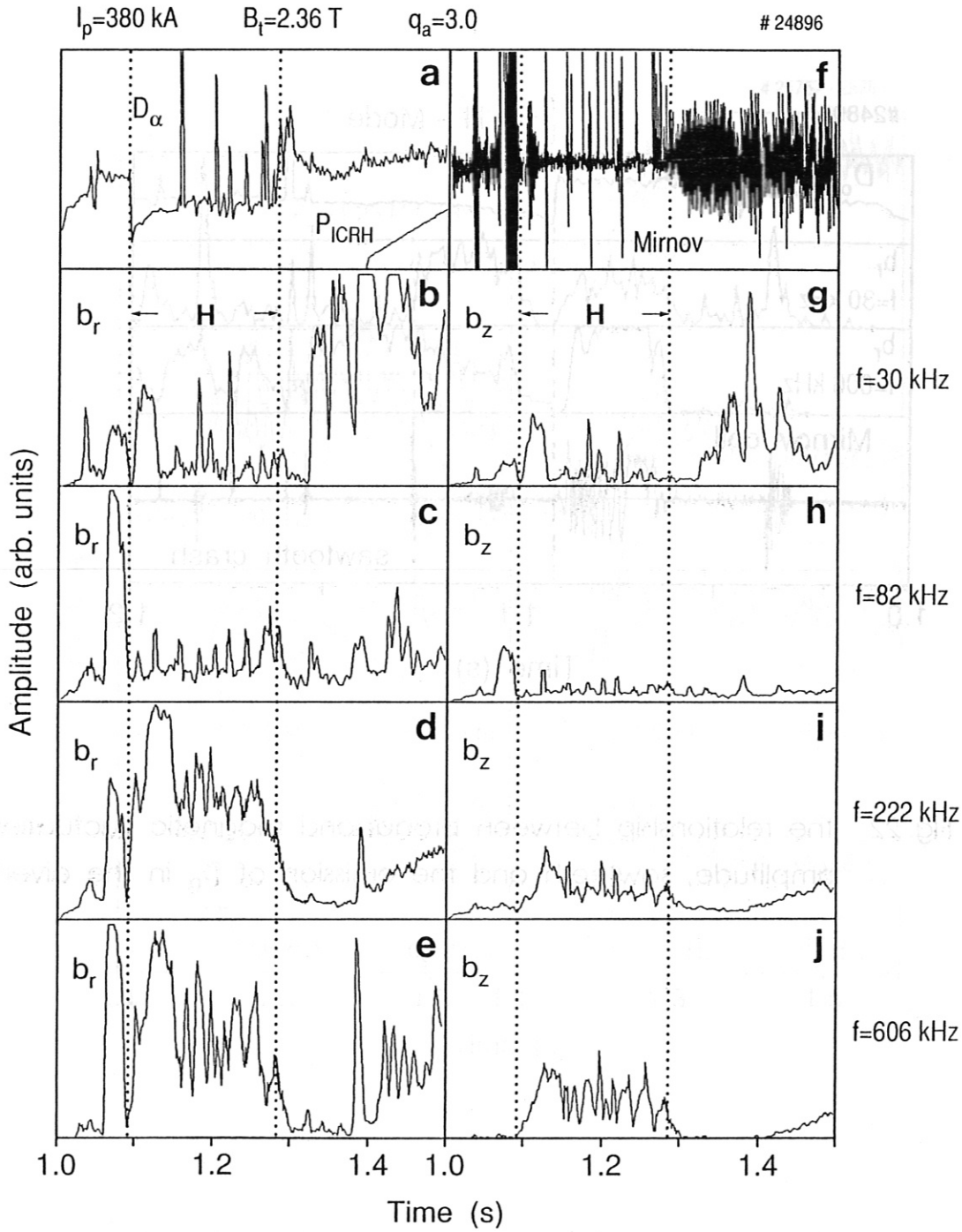

Fig. 21 Frequency dependence of the broadband magnetic fluctuation amplitude in the L to H transition.

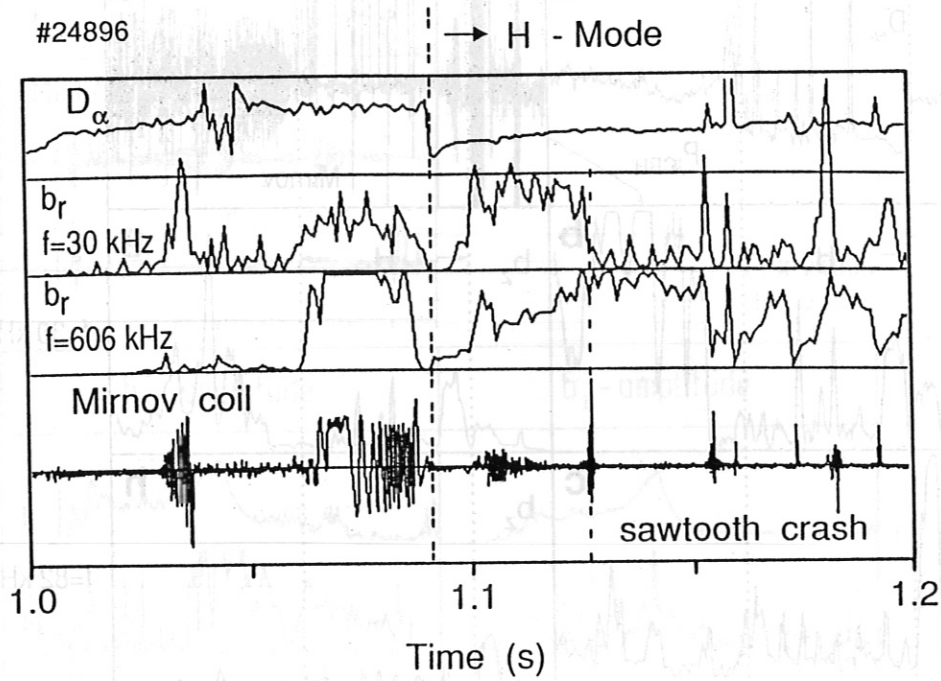

Fig. 22 The relationship between broadband magnetic fluctuation amplitude, sawteeth and the emission of D_α in the divertor.

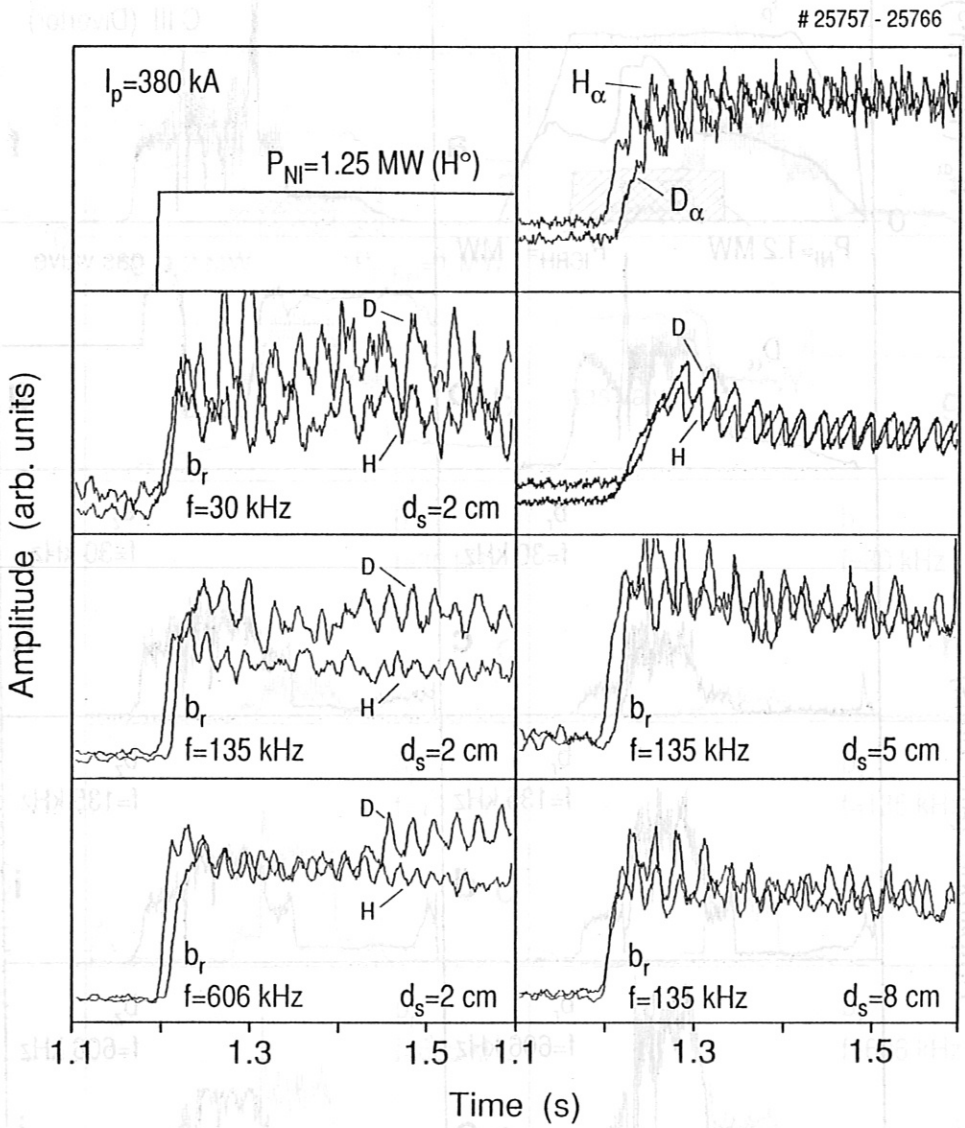

Fig. 23 The dependence of broadband magnetic fluctuation amplitude on the isotope of the filling gas.

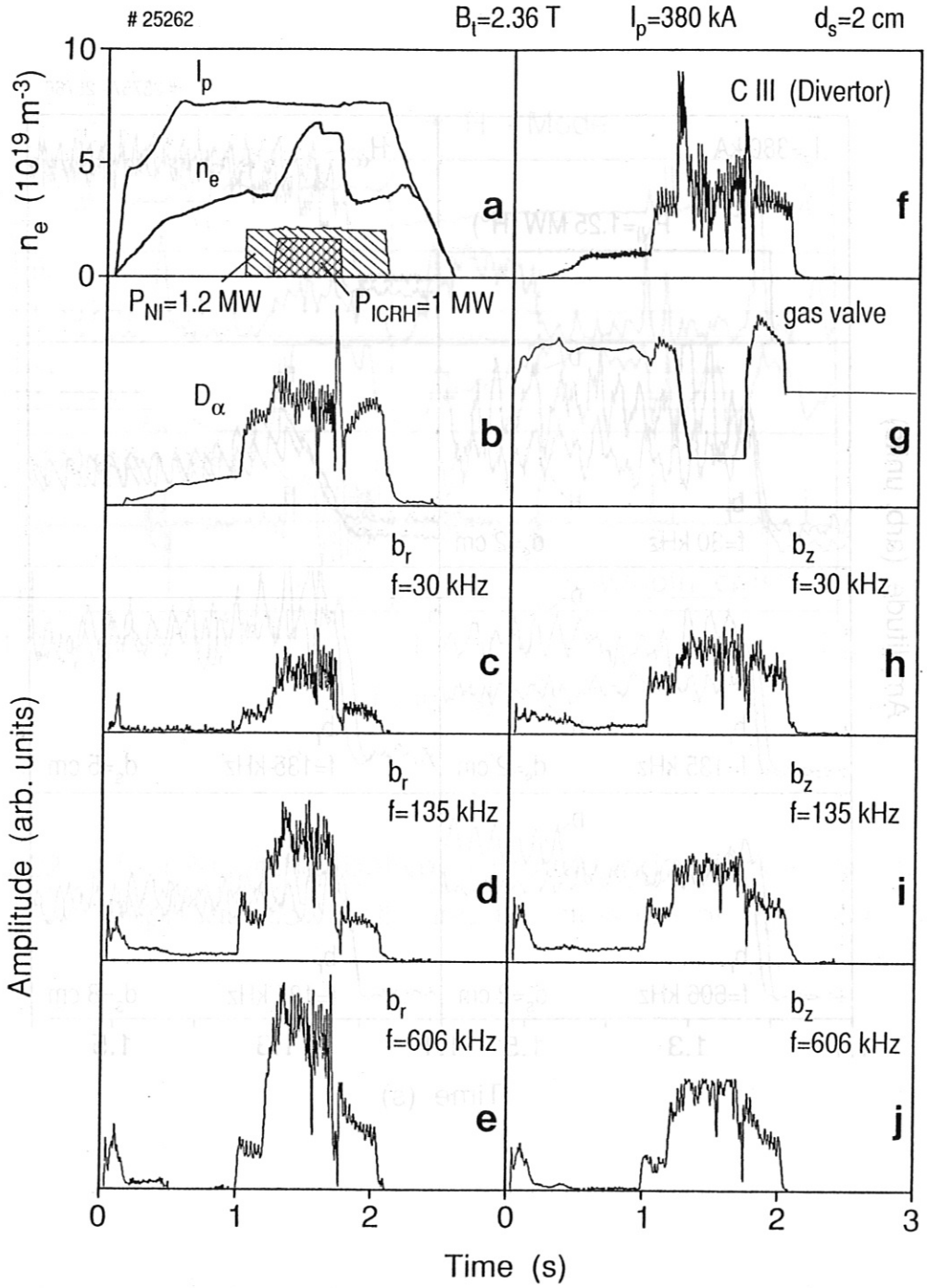

Fig. 24 The frequency dependence of the fluctuation amplitude in an ICRH discharge with d_s = 2 cm.

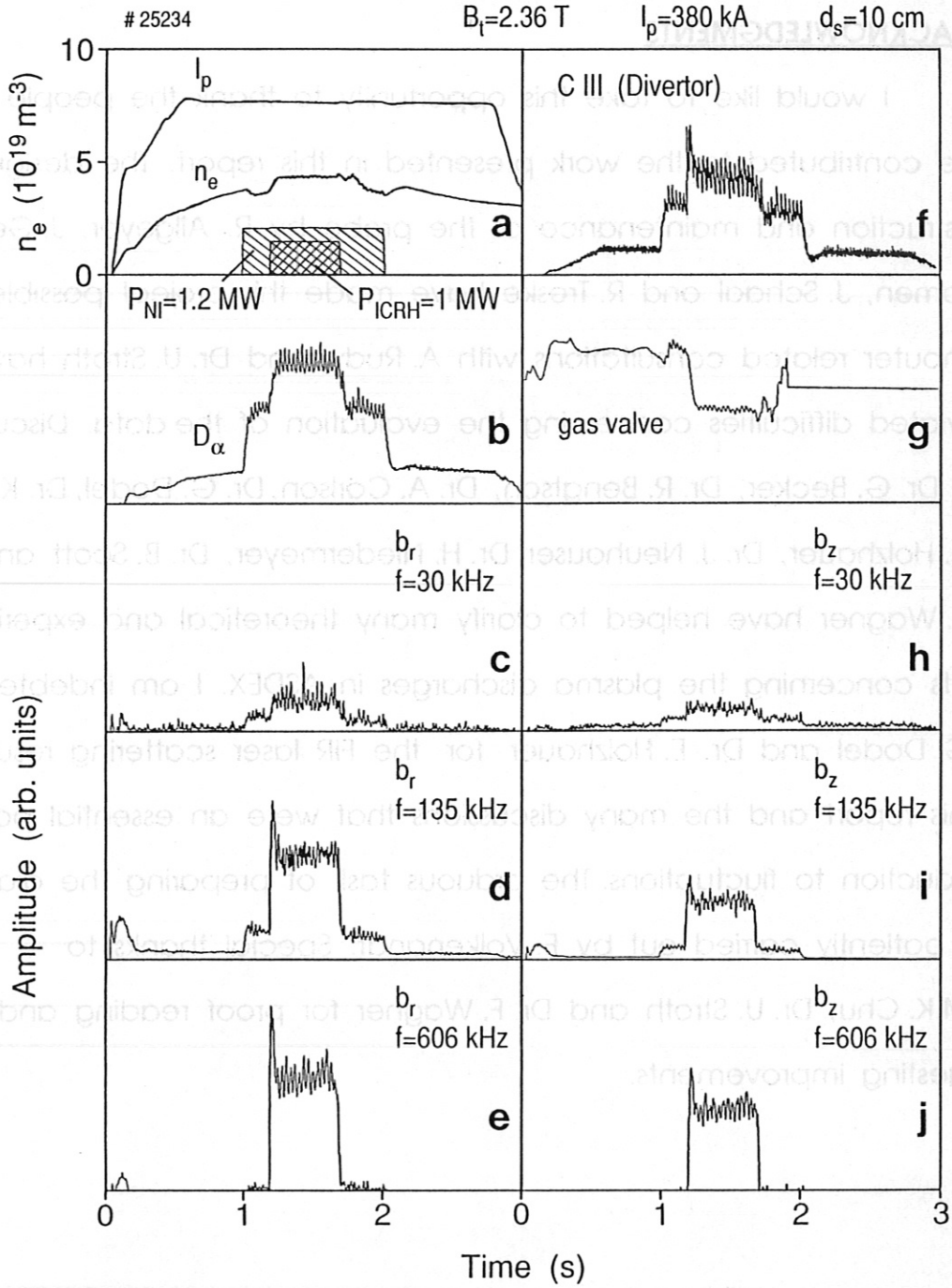

Fig. 25 The frequency dependence of the fluctuation amplitude in an ICRH discharge with d_s = 10 cm.

9. ACKNOWLEDGMENTS

I would like to take this opportunity to thank the people that have contributed to the work presented in this report. The design, construction and maintenance of the probe by R. Allgeyer, J. Gernhardt, R. Komen, J. Schaal and R. Treske have made this project possible. Computer related consultations with A. Rudyj and Dr. U. Stroth have alleviated difficulties concerning the evaluation of the data. Discussions with Dr. G. Becker, Dr. R. Bengtson, Dr. A. Carlson, Dr. G. Dodel, Dr. K. Grassie, Dr. E. Holzhauer, Dr. J. Neuhauser, Dr. H. Niedermeyer, Dr. B. Scott and Dr. F. Wagner have helped to clarify many theoretical and experimental points concerning the plasma discharges in ASDEX. I am indebted to Dr. G. Dodel and Dr. E. Holzhauer for the FIR laser scattering results used in this report and the many discussions that were an essential part of my introduction to fluctuations. The arduous task of preparing the diagrams was patiently carried out by E. Volkenandt. Special thanks to Dr. M.K. Chu, Dr. U. Stroth and Dr. F. Wagner for proof reading and suggesting improvements.